



Short Report

Exome sequencing of two patients in a family with atypical X-linked leukodystrophy

Tsurusaki Y, Okamoto N, Suzuki Y, Doi H, Saitsu H, Miyake N, Matsumoto N. Exome sequencing of two patients in a family with atypical X-linked leukodystrophy.

Clin Genet 2011; 80: 161–166. © John Wiley & Sons A/S, 2011

We encountered a family with two boys similarly showing brain atrophy with reduced white matter, hypoplasia of the brain stem and corpus callosum, spastic paralysis, and severe growth and mental retardation without speaking a word. The phenotype of these patients was not compatible with any known type of syndromic leukodystrophy. Presuming an X-linked disorder, we performed next-generation sequencing (NGS) of the transcripts of the entire X chromosome. A single lane of exome NGS in each patient was sufficient. Six potential mutations were found in both affected boys. Two missense mutations, including c.92T>C (p.V31A) in *LICAM*, were potentially pathogenic, but this remained inconclusive. The other four could be excluded. Because the patients did not show adducted thumbs or hydrocephalus, the *LICAM* change in this family can be interpreted as different scenarios. Personal genome analysis using NGS is certainly powerful, but interpretation of the data can be a substantial challenge requiring a lot of tasks.

Conflict of interest

None of the authors have any conflicts of interest to disclose.

Y Tsurusaki^a, N Okamoto^b,
Y Suzuki^c, H Doi^a, H Saitsu^a,
N Miyake^a and N Matsumoto^a

^aDepartment of Human Genetics, Yokohama City University Graduate School of Medicine, Kanazawa-ku, Yokohama, Japan, and ^bDepartment of Medical Genetics, and ^cDepartment of Pediatric Neurology, Osaka Medical Center and Research Institute for Maternal and Child Health, Murodo-cho, Izumi, Japan

Key words: atypical phenotype – exome sequencing – *L1CAM* – X-linked leukodystrophy

Corresponding author: Naomichi Matsumoto, Department of Human Genetics, Yokohama City University Graduate School of Medicine, 3-9 Fukuura, Kanazawa-ku, Yokohama 236-0004, Japan.
Tel.: +81-45-787-2606;
fax: +81-45-786-5219;
e-mail: naomat@yokohama-cu.ac.jp

Received 4 May 2011, revised and accepted for publication 31 May 2011

Focused/selected gene and genomic characterization has usually been carried out in clinically homogeneous groups of multiple affected samples to make identification of genetic abnormalities more efficient. Microarrays and next-generation sequencing (NGS) have provided new avenues for human genetic research (1–6). Using such new technologies, researchers are able to analyze small numbers of patients on a genome-wide scale. Even very rare cases (such as when only a few compatible patients are available or atypical patients showing no similar phenotypes) can be realistic targets of genetic research, as the new technologies can identify aberrations in a single gene from within virtually the whole genome; this could not be achieved with conventional techniques.

We encountered a family with two affected males showing atypical leukodystrophy. The phenotype of these patients did not match any known type of syndromic leukodystrophy. Because we presumed that abnormality of an X-linked gene caused the atypical leukodystrophy in this family, we performed exome sequencing of most of the X-chromosome transcripts and identified an unexpected gene mutation in these patients.

Materials and methods

A family with atypical X-linked leukodystrophy

Two brothers, II-1 currently aged 19 years and II-2 currently aged 17 years, who have unrelated healthy parents, presented with similar clinical

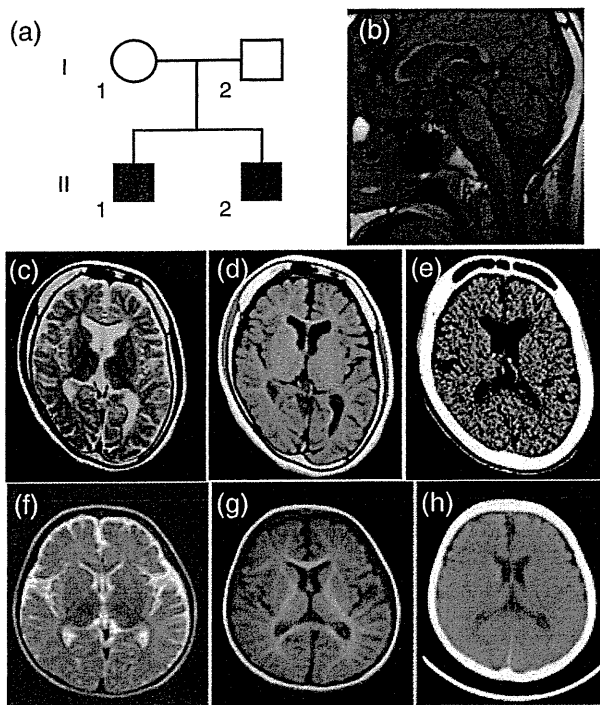


Fig. 1. Clinical features of the family. Familial pedigree (a). Brain magnetic resonance imaging (MRI) (b: T1-weighted image, c: T2-weighted image, d: T1-weighted image) of individual II-1 at 16 years old showing hypoplasia of the white matter, the brain stem and the corpus callosum. Brain computed tomographic (CT) images of individual II-1 at 19 years old (e) indicating a thick calvarium with enlarged frontal sinus as well as calcification of the choroid plexus in the atrophic brain. Brain MRI (f: T2-weighted image, g: T1-weighted image) of individual II-2 at 2 years old, also displaying hypoplasia of the white matter. Brain CT image of individual II-2 at 5 years old (h), also showing a thick calvarium.

features. Their mother did not show any neurological abnormalities (Fig. 1a).

Patient II-1

Patient II-1's birth weight was 2840 g at 40 weeks of gestational age. He had congenital nystagmus. He sat unsupported at 7 months old but after this his developmental milestones were delayed. He could creep at 18 months old. Spastic paralysis, especially in the lower extremities, became apparent. He was unable to stand unsupported. His mental development was severely delayed, and he needed special education from elementary school. He had suffered generalized epileptic seizures since he was 10 years old. He was confined to a wheelchair. He had severe mental retardation without speaking a word. His developmental quotient (DQ) at 9 years old was 19 by the Japanese standard method. Severe growth retardation [143 cm (<3%), 24 kg (<3%), occipitofrontal head circumference 49 cm (<3%) at 19 years] was also

noted. He did not have dysmorphic features. Blood analysis revealed microcytic anemia [hemoglobin (Hb) 13.4 g/dl, mean corpuscular volume (MCV) (of red blood cell) 70.4 fl (normal: 89–99 fl), mean corpuscular hemoglobin (MCH) (of red blood cell) 23.1 pg (normal: 29–35 pg)] without any evidence of hemolysis or iron deficiency. Hormonal examination indicated that the levels of luteinizing hormone, follicle-stimulating hormone, and thyroid-stimulating hormone were all low [0.9 mIU/ml (normal: 1.2–8.0 mIU/ml), 2.5 mIU/ml (normal: 2.3–15.1 mIU/ml), <0.01 μ IU/ml (normal: 0.5–5.0 μ IU/ml), respectively]. He showed delayed puberty with small testes. Pubic hair only appeared at 17 years old. His bone age at 18 years old was 12.6 years (67%). Brain magnetic resonance imaging (MRI) at 16 years old revealed brain atrophy associated with reduced white matter and hypoplasia of the brain stem and the corpus callosum (Fig. 1b–d). No hydrocephalus or adducted thumb was observed. Brain computed tomography (CT) at 19 years old showed a thick calvarium with enlarged frontal sinus as well as calcification of the cerebellar tentorium and the choroid plexus (Fig. 1e).

Patient II-2

Patient II-2's birth weight was 2910 g at 37 weeks of gestational age. Developmental delay was apparent since he was 10 months old. Spastic paralysis (especially in the lower extremities), confinement to a wheelchair, severe mental retardation without speaking a word (DQ = 5 at 17 years old), and severe growth retardation [130 cm (<3%) and 27 kg (<3%) at 17 years] were phenotypes shared with his brother (II-1). Blood analysis revealed microcytic anemia (Hb 12.0 g/dl, MCV 61.1 fl, MCH 19.0 pg) without any evidence of hemolysis or iron deficiency. Hormonal examination indicated that the levels of luteinizing hormone, follicle-stimulating hormone, and thyroid-stimulating hormone were relatively low (1.9 mIU/ml, 4.2 mIU/ml, <0.23 μ IU/ml, respectively). He also showed delayed puberty with small testes. Pubic hair appeared only at 17 years old. His bone age at 17 years old was 11 years (65%). Brain MRI at 2 years old revealed brain atrophy associated with reduced white matter and hypoplasia of the brain stem and corpus callosum (Fig. 1f,g). Brain CT at 5 years old showed a thick calvarium (Fig. 1h). No hydrocephalus or adducted thumb was observed. Most of the clinical features were similar to those of his brother except for the absence of nystagmus in patient II-2.

Genome-wide SNP genotyping

Genome-wide single-nucleotide polymorphism (SNP) genotyping was performed on individuals I-2, II-1, and II-2 using a GeneChip™ Human Mapping 10K Array Xba 142 2.0 (Affymetrix, Inc., Santa Clara, CA), according to the manufacturer's protocols. Mendelian error in the pedigree to exclude conflicted SNPs was checked using GCOS 1.2 (GeneChip Operating Software; Affymetrix) and batch analysis in GTYPE 4.0 (GeneChip Genotyping Analysis Software; Affymetrix), with the default setting for the mapping algorithm. The linked region, with SNP genotypes shared between individuals II-1 and II-2, was checked manually.

Genomic partitioning, short-read sequencing, and sequence alignment

Three micrograms of genomic DNA from the affected brothers (II-1 and II-2) was processed using a SureSelect X Chromosome test kit (1582 transcripts covering 3053 kb) (Agilent Technologies, Santa Clara, CA), according to the manufacturer's instructions. Captured DNAs were analyzed using an Illumina GAIIX (Illumina, Inc., San Diego, CA). We used only one of the eight lanes in the flow cell (Illumina) for paired-end, 76-bp reads per sample. Image analysis and base-calling were performed using sequence control software (SCS) real-time analysis and off-line BASECALLER software v1.8.0 (Illumina). Reads were aligned to the human reference genome (UCSC hg19, NCBI build 37.1) using the ELANDv2 algorithm in CASAVA.v1.7.0 (Illumina). The ELANDv2 algorithm can align 100-bp reads to a reference sequence and split the reads into multiple seeds.

Mapping strategy and variant annotation

Approximately 57.5 million reads from individual II-1 and 71.1 million reads from individual II-2 that passed the quality control (Path Filter) were mapped to the human reference genome using mapping and assembly with quality (MAQ) (7) (Fig. 2). MAQ was able to align 51 720 952 and 65 990 660 reads to the whole genome for individuals II-1 and II-2, respectively; these were then statistically analyzed for coverage using a script created by BITS Co., Ltd. (Tokyo, Japan). SNPs and insertions/deletions were extracted from the alignment data using an original script created by BITS Co., Ltd., along with information on the registered SNPs (dbSNP 131). A consensus quality score of 40 or more was used for the SNP analysis in MAQ. SNPs in MAQ-passed reads were

annotated using the SeattleSeq website (<http://gvs.gs.washington.edu/SeattleSeqAnnotation/>). Variants found by each informatics method were selected in terms of location on chromosome X, unregistered variants (excluding registered SNPs), variants in known genes, variants in coding regions, variants excluding synonymous changes, and variants with an allele frequency of at least 90% (assuming a homozygous mutation). NEXTGENE software v2.0 (SoftGenetics, State College, PA) was also used to analyze the reads, with a default setting. Variants found by both of the informatics methods were selected. The variants found in common between individuals II-1 and II-2 were focused on, and confirmed as true positives by Sanger sequencing of polymerase chain reaction (PCR) products amplified from patient genomic DNA, except for variants within genes at segmental duplications. The pathological significance of the variants was evaluated using four different websites: POLYPHEN (Polymorphism Phenotyping; <http://genetics.bwh.harvard.edu/pph/index.html>), POLYPHEN-2 (<http://genetics.bwh.harvard.edu/pph2/index.shtml>), SIFT (<http://sift.jcvi.org/>) (output values less than 0.05 are deleterious), and MUTATIONTASTER (<http://neurocore.charite.de/MutationTaster/>).

Capillary sequencing

Possible pathological variants were confirmed by Sanger sequencing using an ABI 3500xl or ABI3100 autosequencer (Life Technologies, Carlsbad, CA), following the manufacturer's protocol. Sequencing data were analyzed using SEQUENCHER software (Gene Codes Corporation, Ann Arbor, MI).

Expression studies

The relative mRNA levels of *TMEM187* in cDNA of various fetal and adult human tissues (Human MTC™ Panel I and Human Fetal MTC™ Panel; Clontech, Mountain View, CA) were determined by quantitative real-time reverse transcription–polymerase chain reaction (RT-PCR) using TaqMan gene expression assays (Hs01920894_s1 for *TMEM187* and Hs00357333_g1 for β -actin as a control) (Life Technologies).

Results and discussion

Our coverage analysis indicated that for individuals II-1 and II-2, 79.2% and 78.8%, respectively, of the entire X-chromosome coding sequence (CDS) were completely covered, and 88.5% and 88.5%,

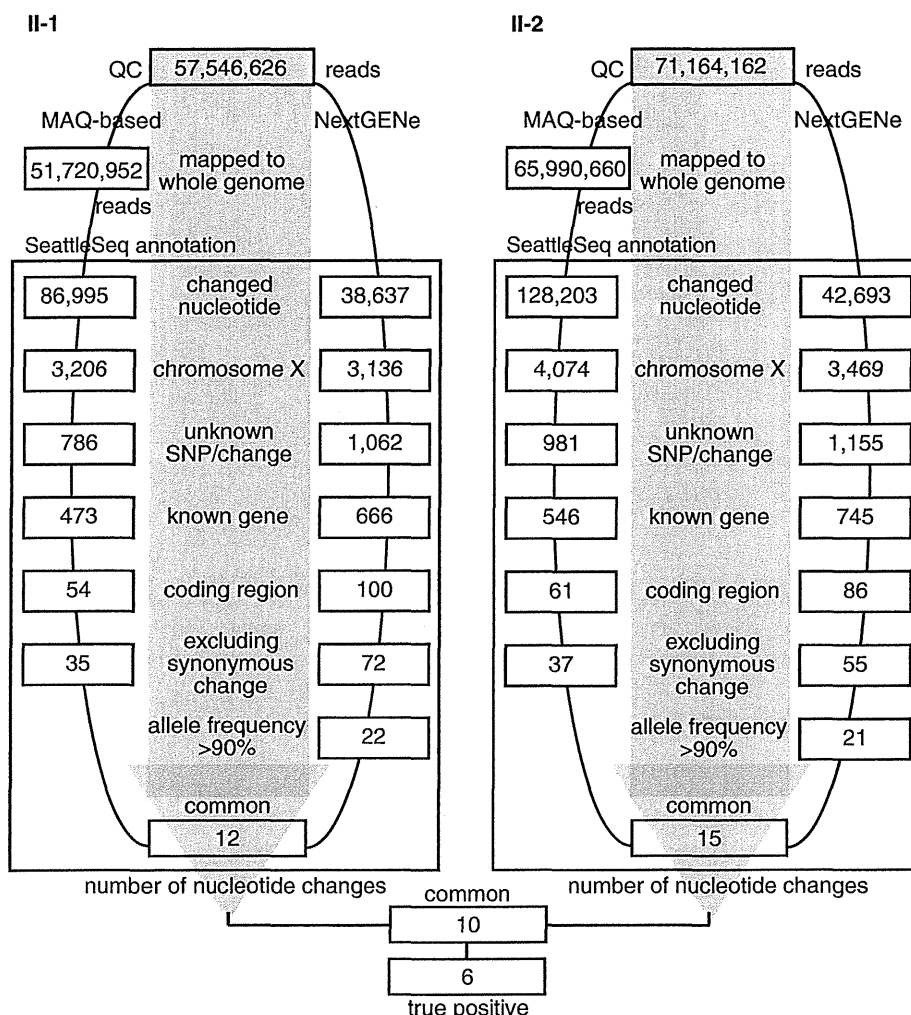


Fig. 2. Flow of informatics analysis. A MAQ-based method and NextGENe analysis were performed in individuals II-1 and II-2. The selection methods employed included variants compared with the human genome reference sequence, variants mapped to chromosome X, unknown variants [excluding registered single-nucleotide polymorphisms (SNPs)], variants in known genes, variants in coding regions, variants excluding synonymous changes, and variants common to the two informatics methods. Finally, the nucleotide changes in common between individuals II-1 and II-2 were focused on as potentially pathogenic mutations. True positive changes were confirmed by capillary sequencing of polymerase chain reaction (PCR) products amplified from genomic DNA.

respectively, of the CDS were at least 90% covered by reads. Using a single lane of sequencing per sample, the coverage with 20 reads or more comprised 89.6% and 89.7% of the CDS, and that with 100 reads or more comprised 87.6% and 89.7% of the CDS in individuals II-1 and II-2, respectively. SNP genotyping indicated that the region from rs727240 to rs721003 (UCSC genome browser hg19 assembly, chromosome X coordinates: 22131639–54454152; 32.2 Mb) was unlinked to the phenotype. Exome sequencing using two informatics methods successfully identified six potentially interesting changes as true positives in the linked region: *FAM123B* (RefSeq Gene ID NM_152424): c.85G>A (p.A29T), *FRMD7* (NM_194277): c.875T>C (p.L292P),

LICAM (NM_000425): c.92T>C (p.V31A), *TME M187* (NM_003492): c.334G>A (p.A112T), *FLNA* (NM_001110556): c.1582G>A (p.V528M), and *LAGE3* (NM_006014): c.395G>A (p.R132Q).

The c.92T>C (p.V31A) variant in *LICAM* was previously found in a patient with Hirschsprung disease, acrocallosal syndrome, and congenital hydrocephalus (8). *LICAM* mutations cause a wide variety of clinical phenotypes: hydrocephalus due to stenosis of the aqueduct of Sylvius (MIM #307000), MASA syndrome (mental retardation, aphasia, shuffling gait, adducted thumb; MIM #303350), and X-linked agenesis of the corpus callosum (MIM #217990). Phenotypic variability, even within a family, has been noted, raising the caution that definite clinical diagnosis in single

Table 1. Characterization of nucleotide changes found by exome sequencing

	<i>FAM123B</i>	<i>FRMD7</i>	<i>L1CAM</i>	<i>TMEM187</i>	<i>FLNA</i>	<i>LAGE3</i>
Change	c.85G>A (p.A29T)	c.875T>C (p.L292P)	c.92T>C (p.V31A)	c.334G>A (p.A112T)	c.1582G>A (p.V528M)	c.395G>A (p.R132Q)
POLYPHEN	Benign	Probably damaging	Benign	Benign	Probably damaging	Benign
POLYPHEN-2	Probably damaging	Probably damaging	Benign	Possibly damaging	Possibly damaging	Possibly damaging
SIFT	0.04	0.02	0.22	0.02	0.04	0.46
MUTATIONTASTER	Polymorphism	Disease causing	Disease causing	Polymorphism	Polymorphism	Polymorphism
Normal female	<u>8/502^a</u>	2/502	2/502	1/502	<u>15/502^a</u>	4/502
Normal male	<u>1/118</u>	0/117	0/118	0/118		<u>1/86</u>
Note		No nystagmus in II-2				

^aIncluding one homozygous female. Underlining means that this result excludes the variant as potentially causative. Grayed shading indicates the variants that could not be excluded; between these two, the *L1CAM* variant is more likely to be causative.

cases is often impossible (9). Phenotypic features compatible with the *L1CAM* mutation in our patients include spastic paralysis, aphasia, severe mental and growth retardation, but atypical leukodystrophy and the absence of adducted thumbs were very rare or exceptional (9). A normal control study found that 2 of 251 normal females were heterozygous for this SNP, but none of 117 normal males carried the variant allele. One of the four web-based analyses of pathological significance (MutationTaster) indicated that this variant would be disease causing, while the others indicated that it would be benign (Table 1). X-linked hydrocephalus due to *L1CAM* mutations occurs in approximately 1/30 000 male births (10). Considering that the *L1CAM* mutation was found in 2/618 control alleles (0.32%), the change may be a rare polymorphism, a mutation causing lethality in the majority of affected males, or a mutation with low penetrance. Because we were unable to exclude this *L1CAM* change, its pathogenic status remains inconclusive.

We next examined c.85G>A in *FAM123B*, c.875T>C in *FRMD7*, c.1582G>A in *FLNA*, and c.395G>A in *LAGE3* in normal controls. The *FAM123B*, *FLNA*, and *LAGE3* variants were excluded as causative because a homozygous change was found in 1 of 251 female controls (*FAM123B* and *FLNA*) or a hemizygous change was found in 1 of 86 normal males (*LAGE3*). However, the thick calvarium in individuals II-1 and II-2 may be influenced by the *FAM123B* change, because it is causative for osteopathia striata with cranial sclerosis, an X-linked dominant disorder (MIM #300373) (11, 12). As the calvarium of the patients' mother having the heterozygous *FAM123B* change was not evaluated by CT, we could not confirm this possibility.

Only 2 of 251 control females carried the c.875T>C variant in *FRMD7* heterozygously, and none of 117 male controls carried this variant; thus, the pathogenicity of the *FRMD7* variant was inconclusive. Other *FRMD7* mutations cause X-linked congenital nystagmus 1 (MIM #310700) (13). However, the nystagmus found in individual II-1 was not observed in individual II-2, indicating that the variant in common between two brothers did not consistently cause nystagmus. Thus, it may not contribute to the phenotype in this family (Table 1).

We also evaluated the c.334G>A variant in *TMEM187*. Only 2 of 251 female controls carried this heterozygous change, and it was not found among 118 male controls. Two of the four programs (POLYPHEN-2 and SIFT) indicated that it would be pathogenic. By Taqman assay, *TMEM187* was ubiquitously expressed in various fetal and adult tissues, including the brain (data not shown), leaving the effect of this mutation on the phenotype in these patients inconclusive (Table 1).

In conclusion, we found two possible but inconclusive variants in this family with two boys affected by atypical leukodystrophy. High-throughput technologies are clearly powerful to detect genomic changes, but evaluation of the data can be very difficult and should be performed cautiously. More knowledge of rare SNPs and mutations is absolutely necessary before any conclusions can be drawn.

Acknowledgements

We would like to thank the patients and their family members for their participation in this study. This work was supported by research grants from the Ministry of Health, Labour and Welfare

Tsurusaki et al.

(to H. S., N. Miyake, and N. Matsumoto), the Japan Science and Technology Agency (to N. Matsumoto), a Grant-in-Aid for Scientific Research from the Japan Society for the Promotion of Science (to N. Matsumoto), and a Grant-in-Aid for Young Scientists from the Japan Society for the Promotion of Science (to H. D., N. Miyake, and H. S.).

References

1. Saitsu H, Kato M, Mizuguchi T et al. De novo mutations in the gene encoding STXBP1 (MUNC18-1) cause early infantile epileptic encephalopathy. *Nat Genet* 2008; 40: 782–788.
2. Check Hayden E. Genomics shifts focus to rare diseases. *Nature* 2009; 461: 458.
3. Biesecker LG. Exome sequencing makes medical genomics a reality. *Nat Genet* 2010; 42: 13–14.
4. Kuhlenbaumer G, Hullmann J, Appenzeller S. Novel genomic techniques open new avenues in the analysis of monogenic disorders. *Hum Mutat* 2011; 32: 144–151.
5. Miyake N, Kosho T, Mizumoto S et al. Loss-of-function mutations of CHST14 in a new type of Ehlers-Danlos syndrome. *Hum Mutat* 2010; 31: 966–974.
6. Ng SB, Bigham AW, Buckingham KJ et al. Exome sequencing identifies MLL2 mutations as a cause of Kabuki syndrome. *Nat Genet* 2010; 42: 790–793.
7. Li H, Ruan J, Durbin R. Mapping short DNA sequencing reads and calling variants using mapping quality scores. *Genome Res* 2008; 18: 1851–1858.
8. Nakakimura S, Sasaki F, Okada T et al. Hirschsprung's disease, acrocallosal syndrome, and congenital hydrocephalus: report of 2 patients and literature review. *J Pediatr Surg* 2008; 43: E13–E17.
9. Rietschel M, Friedl W, Uhlhaas S, Neugebauer M, Heimann D, Zerres K. MASA syndrome: clinical variability and linkage analysis. *Am J Med Genet* 1991; 41: 10–14.
10. Rosenthal A, Jouet M, Kenwrick S. Aberrant splicing of neural cell adhesion molecule L1 mRNA in a family with X-linked hydrocephalus. *Nat Genet* 1992; 2: 107–112.
11. Viot G, Lacombe D, David A et al. Osteopathia striata cranial sclerosis: non-random X-inactivation suggestive of X-linked dominant inheritance. *Am J Med Genet* 2002; 107: 1–4.
12. Jenkins ZA, van Kogelenberg M, Morgan T et al. Germline mutations in WTX cause a sclerosing skeletal dysplasia but do not predispose to tumorigenesis. *Nat Genet* 2009; 41: 95–100.
13. Tarpey P, Thomas S, Sarvananthan N et al. Mutations in FRMD7, a newly identified member of the FERM family, cause X-linked idiopathic congenital nystagmus. *Nat Genet* 2006; 38: 1242–1244.

SMOC1 Is Essential for Ocular and Limb Development in Humans and Mice

Ippei Okada,^{1,14} Haruka Hamanoue,^{1,2,14} Koji Terada,³ Takaya Tohma,⁴ Andre Megarbane,⁵ Eliane Chouery,⁵ Joelle Abou-Ghoch,⁵ Nadine Jalkh,⁵ Ozgur Cogulu,⁶ Ferda Ozkinay,⁶ Kyoji Horie,⁷ Junji Takeda,^{7,8} Tatsuya Furuichi,^{9,10} Shiro Ikegawa,⁹ Kiyomi Nishiyama,¹ Satoko Miyatake,¹ Akira Nishimura,¹ Takeshi Mizuguchi,^{1,15} Norio Niikawa,^{11,12} Fumiki Hirahara,² Tadashi Kaname,¹³ Koh-ichiro Yoshiura,¹² Yoshinori Tsurusaki,¹ Hiroshi Doi,¹ Noriko Miyake,¹ Takahisa Furukawa,³ Naomichi Matsumoto,^{1,*} and Hiroto Saito^{1,*}

Microphthalmia with limb anomalies (MLA) is a rare autosomal-recessive disorder, presenting with anophthalmia or microphthalmia and hand and/or foot malformation. We mapped the MLA locus to 14q24 and successfully identified three homozygous (one nonsense and two splice site) mutations in the SPARC (secreted protein acidic and rich in cysteine)-related modular calcium binding 1 (*SMOC1*) in three families. *Smoc1* is expressed in the developing optic stalk, ventral optic cup, and limbs of mouse embryos. *Smoc1* null mice recapitulated MLA phenotypes, including aplasia or hypoplasia of optic nerves, hypoplastic fibula and bowed tibia, and syndactyly in limbs. A thinned and irregular ganglion cell layer and atrophy of the anteroventral part of the retina were also observed. Soft tissue syndactyly, resulting from inhibited apoptosis, was related to disturbed expression of genes involved in BMP signaling in the interdigital mesenchyme. Our findings indicate that *SMOC1/Smoc1* is essential for ocular and limb development in both humans and mice.

Introduction

Microphthalmia with limb anomalies (MLA [MIM 206920]), also known as Waardenburg anophthalmia syndrome or ophthalmoacromelic syndrome, is a rare autosomal-recessive disorder first described by Waardenburg.¹ It is characterized by ocular anomalies ranging from mild microphthalmia to true anophthalmia and by limb anomalies such as oligodactyly, syndactyly, and synostosis of the 4th and 5th metacarpals.^{2–4} The genetic cause for MLA has remained unknown.

It is widely known that secreted signaling molecules such as Sonic hedgehog (Shh), wingless-type MMTV integration site family (Wnt), transforming growth factor β (Tgf- β), bone morphogenetic proteins (Bmps), and fibroblast growth factor (Fgf) are involved in the development of many organs and tissues, including the eyes and limbs.^{5,6} In particular, mutations in *BMP4* (MIM 112262) have resulted in anophthalmia with systemic manifestations, including polydactyly and/or syndactyly (also known as microphthalmia, syndromic 6, MCOP56 [MIM

607932]),⁷ highlighting importance of BMP signaling in both the developing eye and limb.

SMOC1 (MIM 608488), which encodes SPARC (secreted protein acidic and rich in cysteine)-related modular calcium binding 1, is a member of the SPARC (also known as BM-40) matricellular protein family that modulates cell-matrix interaction by binding to many cell-surface receptors, the extracellular matrix, growth factors, and cytokines.^{8,9} SMOCs are extracellular glycoproteins with five domains: an N-terminal follistatin-like (FS) domain, two thyroglobulin-like (TY) domains, a domain unique to SMOC, and an extracellular calcium-binding (EC) domain.⁹ *SMOC1* is widely expressed in various tissues with localization to basement membranes.^{9,10} Although the biological function of *SMOC1* remains largely unknown, it has been recently reported that *Xenopus smoc* protein, the ortholog of human *SMOC1*, acts as a BMP antagonist,¹¹ suggesting that human *SMOC1* can also modulate BMP signaling.

Here, we demonstrate that *SMOC1* mutations cause MLA. We also show that *Smoc1* null mice recapitulated

¹Department of Human Genetics, Yokohama City University Graduate School of Medicine, 3-9 Fukuura, Kanazawa-ku, Yokohama 236-0004, Japan;

²Department of Obstetrics and Gynecology, Yokohama City University Graduate School of Medicine, 3-9 Fukuura, Kanazawa-ku, Yokohama 236-0004, Japan;

³Department of Developmental Biology, Osaka Bioscience Institute, 6-2-4 Furuedai, Suita, Osaka 565-0874, Japan;

⁴Division of Pediatrics, Okinawa Prefectural Nanbu Medical Center & Children's Medical Center, 118-1 Ikyoku, Arakawa, Haebaru, Okinawa 901-1193, Japan;

⁵Medical Genetics Unit, St. Joseph University, Beirut 1104-2020, Lebanon;

⁶Department of Pediatrics, Ege University Faculty of Medicine, 35100 Bornova-Izmir, Turkey;

⁷Department of Social and Environmental Medicine, Graduate School of Medicine, Osaka University, 2-2 Yamadaoka, Suita, Osaka 565-0871, Japan;

⁸Center for Advanced Science and Innovation, Osaka University, 2-1 Yamadaoka, Suita, Osaka 565-0871, Japan;

⁹Laboratory for Bone and Joint Disease, Center for Genomic Medicine, RIKEN, 4-6-1 Shirokanedai, Minato-ku, Tokyo 108-8639, Japan;

¹⁰Laboratory Animal Facility, Research Center for Medical Sciences, Jikei University School of Medicine, 3-25-8, Nishi-Shimbashi, Minato-ku, Tokyo 105-8461, Japan;

¹¹Research Institute of Personalized Health Sciences, Health Sciences University of Hokkaido, Ishikari-Tobetsu, Hokkaido 061-0293, Japan;

¹²Department of Human Genetics, Nagasaki University Graduate School of Biomedical Sciences, Sakamoto 1-12-4, Nagasaki 852-8523, Japan;

¹³Department of Medical Genetics, University of the Ryukyus Faculty of Medicine, 207 Uehara, Nishihara, Okinawa 903-0215, Japan

¹⁴These authors contributed equally to this work

¹⁵Current address: Laboratory of Biochemistry and Molecular Biology, National Cancer Institute, National Institutes of Health, Building 37, Room 6050, Bethesda, MD 20892, USA

*Correspondence: naomat@yokohama-cu.ac.jp (N.M.), hsaito@yokohama-cu.ac.jp (H.S.)

DOI 10.1016/j.ajhg.2010.11.012. ©2011 by The American Society of Human Genetics. All rights reserved.

MLA phenotypes, indicating that *SMOC1* plays essential roles in both eye and limb development in humans and mice.

Subjects and Methods

Subjects

A total of four families with one or two cases of MLA were analyzed in this study, including three previously reported families (A, B, and C).^{12,13} Family X from Turkey, which has been previously described,¹⁴ was newly recruited to this study. Detailed clinical information of all the patients is available in the literature,^{12,14} and phenotypes of patients with confirmed mutations are summarized in Table S1 (available online). A total of five affected and 16 unaffected members from the four families were analyzed in the linkage study. Genomic DNA was obtained from peripheral-blood leukocytes with the use of QuickGene 610-L (FujiFilm, Tokyo, Japan) after informed consent had been given. Experimental protocols were approved by the institutional review board of Yokohama City University School of Medicine.

SNP Genotyping, and Fine Mapping with Short Tandem Repeat Markers

Whole-genome SNP genotyping, with the use of GeneChip Human Mapping 50K Array XbaI (Affymetrix, Santa Clara, CA), and fine mapping of possible candidate regions, with the use of additional microsatellite markers, were performed as previously described.^{12,15} The list of primers used for fine mapping is presented in Table S2.

Linkage Analysis

Multipoint linkage analyses using aligned SNPs were performed with ALLEGRO software.¹⁶ Two-point linkage analyses of candidate regions were performed with the LINKAGE package MLINK (FASTLINK software, version 5.1). In each program, an autosomal-recessive model of inheritance with complete penetrance and a disease-allele frequency of 0.001 were applied.

Mutation Analysis of Candidate Genes

All coding exons and exon-intron boundaries of *RAD51L1* (MIM 602948), *ACTN1* (MIM 102575), *ERH* (MIM 601191), *SRSF5* (MIM 600914), *DCAF5* (MIM 603812), *COX16*, *EXD2*, *GALNTL1*, *SLC39A9*, *KIAA0247*, *MED6* (MIM 602984), *TTC9* (MIM 610488), *MAP3K9* (MIM 600136), and *SMOC1* (transcript variant 1, GenBank accession number NM_001034852.1) were analyzed in the probands of families A, C, and X. The transcript variant 2 of *SMOC1* (GenBank accession number NM_022137.4) is 3 bp shorter than the variant 1, leading to an in-frame amino acid deletion at position 431. PCR was cycled 35 times at 94°C for 30 s, at 60°C for 30 s, and at 72°C for 30–90 s in a total volume of 20 µl containing 30 ng genomic DNA as a template, 0.5 µM forward and reverse primers, 200 µM each deoxyribonucleotide triphosphate (dNTP), 1 × ExTaq buffer, and 0.25 U ExTaq (Takara). All primers were designed with Primer3 software. Detailed information of primers is available upon request. PCR products were purified with ExoSAP (USB) and sequenced with BigDye Terminator 3.1 (Applied Biosystems) on a 3100 Genetic Analyzer. Sequences of patients were compared to reference genome sequences in the UCSC Genome Browser (February 2009

assembly) with Seqscape software, version 2.1 (Applied Biosystems).

Animals

Smoc1 mutant mice, created with the use of the *Sleeping Beauty* transposon system, have been previously described.¹⁷ Line PV384 was provided by the RIKEN BioResource Center through the National BioResource Project of MEXT, Japan. Three independent mouse lines (no. 1 to no. 3), each with a single insertion in intron 1 of *Smoc1*, were bred as heterozygotes. Lines 1 and 3 were backcrossed for at least four generations to a C57BL/6J background. Line 2 was maintained with a mixed background of C57BL/6J and ICR. We mainly analyzed line 1, but we confirmed similar phenotypes in lines 2 and 3. Animals were housed in accordance with protocols approved by the Institutional Animal Care and Use Committee at Yokohama City University, School of Medicine. PCR genotyping of mice was performed with the use of genomic DNA from yolk-sac, ear, or tail biopsies. The following primers were used: PV384-WF, 5'-AAAGGCTGGAATTGTTTGA-3'; PV384-WR, 5'-TGCAGCTGAACTGTCTCTCC-3'; PV384-MF, 5'-TGTCCCTAACTGACTTGCCAAA-3'. The PV384-WF/PV384-WR primers amplified a 441 bp wild-type (WT) product, and the PV384-MF/PV384-WR primers amplified a 218 bp mutant product.

Southern Hybridization

Genomic DNA was extracted from livers or tail biopsies of PV384 heterozygous (*Smoc1*^{Tp/+}) mice via standard protocols. The gene-trap insertions were analyzed by Southern hybridization with the use of 10 µg of *SacI*-, *NdeI*-, *BglII*-, and *EcoRI*-digested DNA. The probe (451 bp), which hybridized to the internal ribosome entry site (IRES) in the gene-trap vector, was synthesized with the DIG PCR Probe Synthesis Kit (Roche) with the use of the following primers: 5'-CTAACGTTACTGGCCGAAGC-3' and 5'-CCCAGATCAGATCCCATACAA-3'. Hybridization, washing, and detection of probes were performed according to the manufacturer's protocol. Images were captured with the FluorChem system (Alpha Innotech).

Cloning of Gene-Trap Insertion Sites

After identification of aberrant DNA fragments by Southern hybridization, *NdeI*-, *SacI*-, and *EcoRI*-digested DNA from PV384 mice was fractionated by electrophoresis, and appropriately sized fragments containing *Oli1* (*other locus 1*), *Oli2*, and *Oli3* were isolated with a QIAEXII Gel Extraction Kit (QIAGEN). The isolated DNA was self-ligated by Ligation High ver.2 (Toyobo), precipitated with ethanol, and dissolved in 20 µl EB buffer (QIAGEN). Inverse PCR was performed in 25 µl reactions, containing 2 µl ligated DNA, 1 × PCR buffer for KOD FX, 0.4 mM each dNTP, 0.5 µM each primer, and 0.5 U KOD FX DNA polymerase (Toyobo). Primers common to *Oli1*, *Oli2*, and *Oli3* were as follows: Inv-F, 5'-ATCGCCAGTTCTGTATGAACGGTCTGGTCTT-3'; Inv-R, 5'-CCCTCTTACGTGCCAGCCATCTTAGAGATAC-3'. Confirmatory PCR of gene-trap insertion sites for *Oli1*, *Oli2*, and *Oli3* loci was performed with the use of the following primers: *Oli1*-F, 5'-GAGTGGTATTCA TTGGATTCTGCTGAT-3'; *Oli2*-F, 5'-AAATCCAGCTGGCCAACAGACTAAG-3'; *Oli3*-F, 5'-TTGCCGGGTAGACTCTATCAAGAACCA-3'; TBAL-R, 5'-CTTGTGTCATGCACAAAGTAGATGTC-3'. Primer sets of *Oli1*-F/TBAL-R, *Oli2*-F/TBAL-R, and *Oli3*-F/TBAL-R could amplify 175 bp, 607 bp, and 767 bp products, respectively. These PCR primer pairs were also used for genotyping of mice harboring a single insertion at the *Smoc1* locus.

Confirmation of Promoter- and Poly(A)-Trapped Transcripts

Whole embryos at embryonic day 10.5 (E10.5) and E11.5 were stored in RNAlater solution (QIAGEN). Total RNA was extracted from WT, *Smoc1*^{Tp/+}, and *Smoc1*^{Tp/Tp} embryos with the use of RNeasy Plus Mini (QIAGEN). One microgram total RNA was subjected to reverse transcription with the use of a PrimeScript 1st Strand Synthesis Kit with random hexamers (Takara). A control reaction with no reverse transcriptase was included in each experiment. PCR was performed in 20 μ l reactions, containing 1 μ l cDNA, 1 \times PCR Buffer for KOD FX, 0.4 mM each dNTP, 0.3 μ M each primer, and 0.4 U KOD FX (Toyobo). Primers used are listed below: *Smoc1*-F, 5'-GTCCCCACCTCCCCAAGTGCTTTGA-3'; *LacZ*-R, 5'-TGCCAAAAGACGGCAATATGGTGGAAA-3'; *GFP*-F, 5'-T CACATGGTCTGCTGGAGTTCGTGAC-3'; *Smoc1*-R, 5'-ACACT TGCTCTGGCCAGCATCTTTCAT-3'. Primer sets of *Smoc1*-F/*Smoc1*-R, *Smoc1*-F/*LacZ*-R, and *GFP*-F/*Smoc1*-R could amplify native *Smoc1* (366 bp), promoter-trapped transcripts (Tp-*LacZ*, 500 bp) and poly(A)-trapped transcripts (Tp-*GFP*, 308 bp), respectively. The PCR conditions were 98°C for 10 s, 68°C for 1 min, for 30 cycles. Primers for *ACTB*¹⁸ were used as an internal control. PCR for *ACTB* was cycled 20 times at 94°C for 20 s, 60°C for 20 s, and 72°C for 30 s in a total volume of 10 μ l containing 0.5 μ l cDNA, 0.4 μ M each primer, 0.2 mM each dNTP, 1 \times ExTaq buffer, and 0.5 U ExTaq HS (Takara). All PCR products were electrophoresed on 2% agarose gels.

In Situ Hybridization

Embryos were collected between E9.5 and E13.5. Whole-mount in situ hybridization was carried out as previously described.^{19,20} Two fragments of *Smoc1* cDNA were obtained as probes by RT-PCR, with the use of total RNA extracted from livers of E16.5 mouse embryos, and subcloned into pCR4-TOPO (Invitrogen). Primer sequences were as follows: probe 1-F, 5'-GTCTGCTCAGCCCC ACT-3'; probe 1-R, 5'-CCTGAACCATGTCTGTGGT-3'; probe P-F, 5'-CAGGAACAGGAAAGGGAAGA-3'; probe P-R, 5'-AAGGGAAA ACCACACAGCAC-3'. PCR products were 1023 bp and 1578 bp, corresponding to nucleotide positions 275–1297 and 1849–3426 of the mouse *Smoc1* cDNA (GenBank accession number NM_001146217.1), respectively. The cDNA fragment amplified with probe P-F and probe P-R primers was identical to the probe used in a previous report.²¹ Digoxigenin-labeled sense and antisense riboprobes were synthesized with the use of a digoxigenin RNA labeling kit (Roche). These two different antisense probes demonstrated identical staining patterns, and the control sense probes showed no staining. The expression pattern was confirmed with more than three embryos. In addition, the following probes were used: *Bmp2* (gift from Y. Takahashi),²² *Sox9* (gift from A. Yamada),²² *Bmp7* (gift from E.J. Robertson), and *Msx2* (gift from Dr. R.E. Maxson, Jr). The numbers of embryos examined were as follows (numerical quantity for WT, *Smoc1*^{Tp/+}, and *Smoc1*^{Tp/Tp}, respectively, shown in parentheses): *Msx2* (2, 1, 3) at E11.5; *Bmp2* (3, 0, 3), *Bmp7* (3, 0, 3), *Msx2* (3, 0, 3), and *Sox9* (2, 1, 3) at E12.5; *Bmp2* (1, 2, 3), *Bmp7* (2, 1, 3), *Msx2* (1, 2, 3), and *Sox9* (1, 3, 4) at E13.5. Stained embryos were cleared in glycerol to enable images to be produced with a VHX-1000 digital microscope (Keyence).

Histology

Heads of embryos and newborns were fixed overnight in 4% paraformaldehyde in PBS at 4°C. These embryos were then washed in PBS. Frozen samples were serially sectioned at 16 μ m (E14.5) and 20 μ m (P0). The numbers of eyes examined (WT, *Smoc1*^{Tp/+},

Smoc1^{Tp/Tp}) were as follows: coronally sectioned at E14.5 (8, 10, 12), coronally sectioned at P0 (8, 10, 6), horizontally sectioned at P0 (2, 2, 4). For evaluation of ventral atrophy of the retina, only the coronally sectioned eyes were used. TB staining was performed according to standard protocols. Forelimbs of mice were fixed in 4% paraformaldehyde in PBS, decalcified in 10% EDTA, and embedded in paraffin. Forelimbs were serially sectioned at 4 μ m and stained with hematoxylin and eosin.

Evaluation of Optic Nerve Diameter

The palatine and orbital bones were carefully removed to expose the optic chiasm and optic nerve. During the dissection process, 4% paraformaldehyde in PBS was frequently applied onto the gaps between the bone and optic nerve. Xylene cyanol was applied to enhance the outline of optic nerves at postnatal day 0 (P0). Photographs of optic nerves were taken with a VHX-1000 digital microscope, and the diameter was measured for right and left optic nerves with the bundled software included with the VHX-1000 instrument.

Skeletal Staining

For skeletal preparations, mice were fixed in 99.5% ethanol after removal of the skin and viscera. Cartilage tissues were stained with 0.015% alcian blue and 20% acetic acid in 75% ethanol for three days at 37°C. After dehydration with 99.5% ethanol for three days, bones were stained with 0.002% alizarin red in 1% KOH. Then skeletons were cleared in 1% KOH for several weeks. For P14 mice, soft tissues were dissolved in 2% KOH before alizarin red staining.

Nile Blue Staining

For the study of apoptosis of hindlimbs at E13.5 and E14.5, Nile blue (NB) staining was performed on the basis of a previously described protocol,²³ except that staining was performed at 37°C (not room temperature). Apoptosis was determined by NB-stained (deceased) cells. After rinsing in Tyrode solution, hindlimbs of control (WT and heterozygous littermates) and homozygous mice were evaluated. Photographs of dorsal aspects were taken with a VHX-1000 digital microscope. Experiments were repeated three times, and reproducible representative results are presented.

Statistical Analysis

Statistical analyses were performed with the use of non-repeated-measures ANOVA followed by Dunnett's post hoc test. The results are given as mean \pm standard deviation, and the threshold p value for statistical significance was 0.01.

Results

Identification of Homozygous *SMOC1* Mutations

We have previously mapped the MLA locus to a 422 kb region at 10p11.23 by analyzing three families (one Japanese family [A] and two Lebanese families [B and C]). This region contained only one gene, *MPP7*, in which no mutations were found.¹² After a new Turkish family (X) was added to the analysis, the MLA locus was again searched by homozygosity mapping to the consanguineous families (X, B, and C) and haplotype mapping to family A for detection of compound-heterozygous mutations; however, we could not detect any common regions

among the four families. We then focused on identifying common regions in any three of the four families to allow for locus heterogeneity (Table S3).

A locus at 14q24.1-q24.2, which showed the highest LOD score (3.936) among the candidate regions larger than 2.0 Mb, was highlighted among families A, C, and X. This locus was analyzed with the use of additional microsatellite markers, and a 3.0 Mb region containing 24 genes was identified (Figures 1A and 1B). A total of 14 genes were sequenced, and homozygous mutations were found in *SMOC1*: c.718C>T (p.Gln240X) in family A, c.664+1G>A in family C, and c.378+1G>A in family X (Figures 1C and 1D). All of these homozygous mutations were cosegregated with the disease phenotype, and the parents of the individuals with these mutations were heterozygous carriers (Figure 1C). We could not find any mutations in *SMOC1* in family B, in which MLA is unlinked to the 14q24.1-q24.2 locus. Interestingly, in family A haplotypes of paternal and maternal alleles, each having the same mutation, are completely different (data not shown), suggesting that the same mutation may have occurred in separate events. The c.718C>T mutation was not detected in 289 healthy Japanese controls, including 100 Okinawa islanders. The other two mutations were not detected in ethnically matched controls (54 Lebanese and 99 Turkish subjects, respectively), nor in 289 Japanese controls. The two splice-donor-site mutations (c.664+1G>A and c.378+1G>A) are predicted to abolish a donor site, as predicted by ESE-finder, NetGene2, HSF2.4.1, SpliceView, and BDGP analysis (Table S4). Thus, the three mutations are likely to lead to a loss of functional *SMOC1*.

***Smoc1* Expression in the Developing Eye and Limb in Mice**

For the examination of *Smoc1* expression in the developing eye and limb, whole-mount in situ hybridization of mouse embryos was performed. *Smoc1* was expressed in the forebrain, midbrain, hindbrain, pharyngeal arch, somites, and forelimb buds at E9.5 (Figure 2A). At E10.5, *Smoc1* expression was observed in the optic stalk (Figure 2B), and at E11.5, expression was localized to the closure site of the optic cup (Figure 2C). Expression of *Smoc1* in developing limbs between E10.5 and E11.5 was observed in both dorsal and ventral regions, with a broader pattern of expression in dorsal regions, but expression was not detected in the most anterior, posterior, and distal parts of limb buds (Figures 2D and 2E). Expression coinciding with chondrogenic condensation was observed at E12.5 (Figure 2F), and expression then became restricted to future synovial joint regions at E13.5 (Figure 2G). This dynamic expression suggests that *Smoc1* plays a critical role in ocular and limb development.

Ocular and Limb Anomalies in *Smoc1* Null Mice

To investigate the pathological basis of MLA due to the loss of *SMOC1* function, we obtained *Smoc1* mutant

mice, PV384.¹⁷ PV384 mice possess gene-trap insertions in the *Smoc1* locus and in three other loci. After PV384 mice were bred with C57BL/6J or ICR mice, we obtained three independent lines (no. 1 to no. 3), each with a sole insertion in intron 1 of *Smoc1* (Figure S1). We mainly analyzed line 1, but we confirmed similar phenotypes in lines 2 and 3. Heterozygous mutant mice (*Smoc1*^{TP/+}) were healthy and fertile. Homozygous mice (*Smoc1*^{TP/TP}) were null mutants, as they showed no native transcript of *Smoc1* (Figure S1E). Homozygous mice were viable at P0; however, they did not survive beyond the first 3 wks of life (Figure 3B). Their growth was retarded in comparison to WT and heterozygous littermates at P0 and P14 (Figures 3A and 3C). Developmental defects in eyes and optic nerves were evident at E14.5. Homozygous mice had relatively small eyes, and histological examinations revealed aplasia or hypoplasia of optic nerves (in 10 of 12 optic nerves), atrophy of the anteroventral part of the retina (in 11 of 12 eyes), and extension of the retinal pigmented epithelium (RPE) to the optic nerve (in 10 of 12 eyes) (Figures 3D–3I). These abnormalities were also observed at P0 (aplasia or hypoplasia of optic nerves [in 7 of 10 optic nerves], retinal atrophy [in 6 of 6 eyes], and RPE extension [in 3 of 6 eyes with identifiable optic nerves]) (Figures 3J–3M). WT or heterozygous littermates did not show any such abnormalities, except that a few eyes of heterozygous mice showed extension of the RPE at E14.5, but not at P0 (in 2 of 10 and 0 of 12 eyes, respectively). Toluidine blue (TB) staining showed ganglion cell layers that were thinned and irregular to varying degrees in homozygous mice, suggesting a reduced number of retinal ganglion cells (Figures 3J–3K'). Thus, *Smoc1* is required for axon sprouting, elongation, or maintenance of retinal ganglion cells.²⁴ Hypoplasia of optic nerves was further quantitatively confirmed by macroscopic examination: the average diameter of optic nerves of homozygous mice was significantly smaller than that of WT and heterozygous littermates at P0 and P14 (Figures 3L–3Q). These data clearly demonstrate that loss of *Smoc1* in mice affects development of the body, retina, and optic nerves, in a manner similar to that seen in MLA patients.^{3,4}

Newborn homozygous mice could be readily identified by their hindlimb syndactyly and pes valgus, whereas no abnormalities were observed in WT and heterozygous pups (Figure 4 and Table 1). Interestingly, the severity of syndactyly varied between mouse lines: line 1 exclusively showed soft tissue syndactyly, whereas line 2 frequently showed four digits (Figures 4F and 4J). Skeletal preparations with alcian blue and alizarin red revealed that the foot with four digits had four phalanx and five metatarsals with fusion to each other (Figure 4K). Thus the *Smoc1* null mutation resulted in a spectrum of phenotypes, from soft tissue syndactyly to four fused digits, probably due to different genetic backgrounds. Bowed tibiae and hypoplastic fibulae were also consistently observed in homozygous mice (Figures 4H and 4L). The articulation between

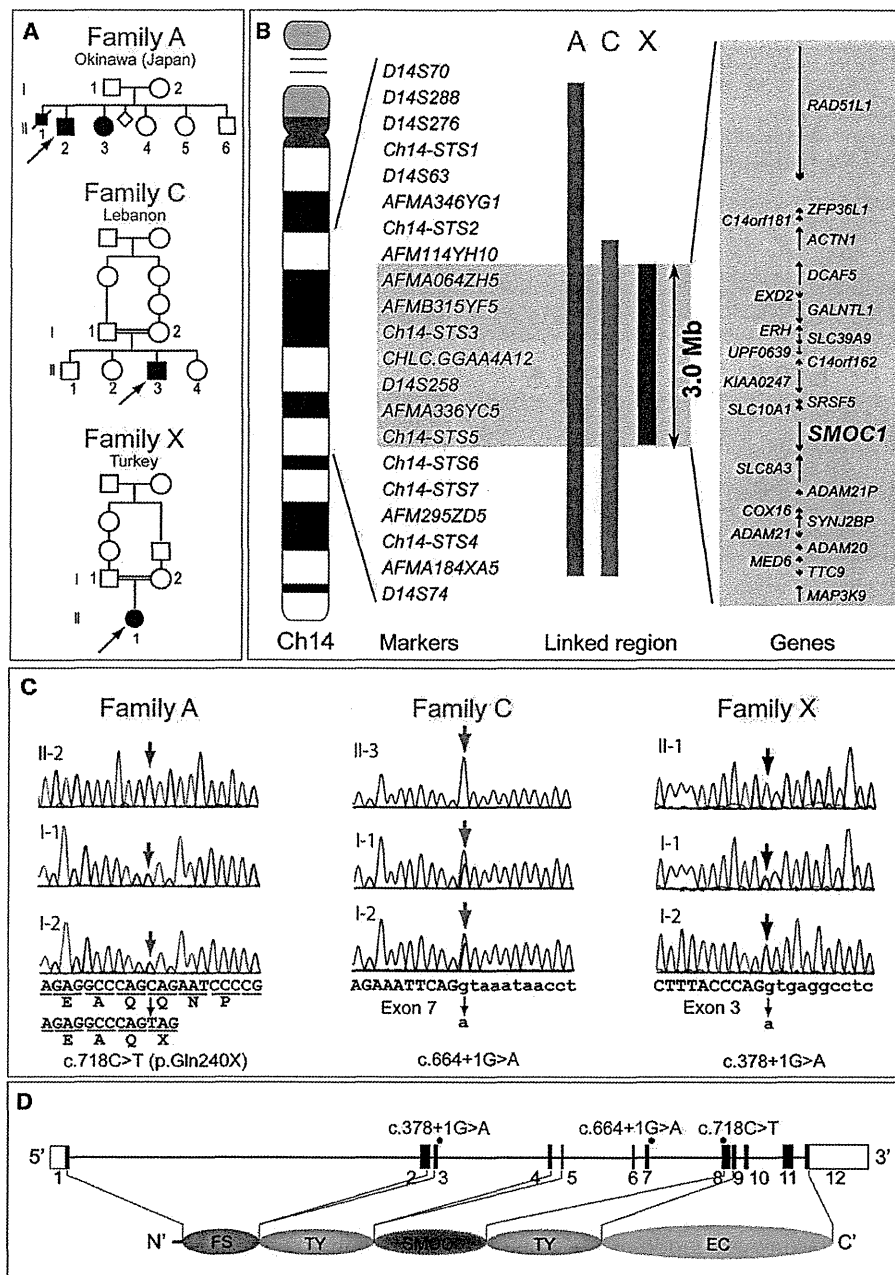


Figure 1. Genetic Analysis of Three Families with Members Affected by Microphthalmia with Limb Anomalies

(A) Pedigrees of the three families.

(B) Linkage analysis with SNPs and microsatellite markers on chromosome 14. From left to right: chromosome ideogram, genetic markers, linked regions of the three families, and genes mapped to the shortest overlapping linked region (between *AFM114YH10* and *Ch14-STS6* [UCSC coordinates, Feb. 2009: chromosome 14: 68,388,190–71,347,908 bp]).

(C) Sequences of mutations identified in each family. Affected patients in family A have a homozygous nonsense mutation (c.718C>T). Patients in families C and X have distinct homozygous splice-donor site mutations (c.664+1G>A and c.378+1G>A, respectively). For all mutations, parents of affected patients are heterozygous carriers, without exception. Sequences of the exon and intron are presented in upper and lower cases, respectively.

(D) At the top is a depiction of a schematic representation of *SMOC1* consisting of 12 exons (UTR and coding exons are indicated by open and filled rectangles, respectively). The locations of three mutations are indicated by red dots. At the bottom, the functional domains of *SMOC1* are depicted. Abbreviations are as follows: FS, the follistatin-like domain; TY, the thyroglobulin-like domain; SMOC, the domain unique to SMOC; and EC, the extracellular calcium-binding domain.

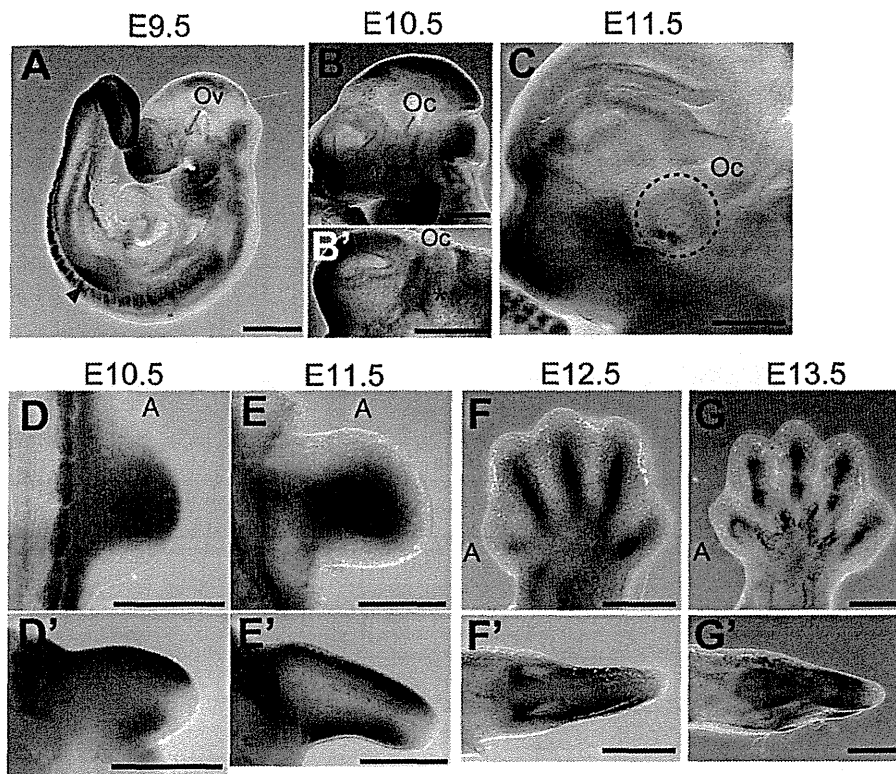


Figure 2. *Smoc1* Expression in Mouse Embryos

Lateral views of embryos (A–C) and a ventral view of the left part of the head (B', lateral view is shown at the top).

(A) At E9.5, *Smoc1* was expressed in the forebrain, midbrain, hindbrain, pharyngeal arch, somites, and forelimb buds (magenta arrow-head), but not in the optic vesicle (Ov, blue arrow).

(B and B') Expression in the optic stalk became evident at E10.5 (magenta asterisks), but was not evident in the optic cup (Oc, blue arrow).

(C) Expression was restricted to the closure site of the optic cup (dashed circle) at E11.5.

(D–G) Dorsal and (D'–G') posterior view of the right hindlimbs (dorsal view is shown at the top in D'–G'). The anterior side is indicated by an A. (D and D') At E10.5, *Smoc1* was more widely expressed in the dorsal part of the limb bud than in the ventral part. *Smoc1* expression is undetected in the most anterior, posterior, and distal parts of the limb bud. (E and E') At E11.5, ventral expression was broader than that in the previous stage. (F and F') At E12.5, expression was detected in areas consistent with chondrogenic condensation. (G and G') At E13.5, *Smoc1* expression became restricted to future joint regions. Scale bar represents 500 μm .

tibia/fibula and calcanea of homozygous mice appeared malpositioned (Figures 4G and 4K), which might contribute to pes valgus. At P14, soft tissue syndactyly was also evident in most forelimbs of homozygous mice (Figures 4M–4O). Moreover, hindlimbs of homozygous mice showed synostosis between the 4th and 5th metatarsals (Figure 4T), which is observed in both the hands and the feet of MLA patients. Thus, many limb anomalies of MLA patients were recapitulated in *Smoc1* null mice (Table S1).

Reduced Interdigital Apoptosis and Disturbed BMP Signaling

Among the various abnormalities caused by loss of *Smoc1* function, we focused on soft tissue syndactyly, which was commonly observed in both fore- and hindlimbs of null mutants. It is possible that the syndactyly is caused by failed apoptotic regression of the interdigital mesenchyme. To examine this hypothesis, hindlimbs were stained with NB sulfate at E13.5 and E14.5, the time

when interdigital apoptosis is most evident. In control embryos (WT and heterozygous littermates), NB-stained apoptotic cells were identified in the interdigital mesenchyme, where regression of the interdigital webbing occurs in the distal region (Figures 5A and 5C). By contrast, the number of apoptotic cells in the mesenchyme between digits 2 and 3 and digits 3 and 4 was dramatically reduced in homozygous mice at E13.5 and E14.5, along with persistent webbing in the distal region (Figures 5B and 5D, magenta asterisk). BMP signaling is involved in apoptosis of the interdigital mesenchyme.^{25,26} *Bmp2*, *Bmp7*, and *Msx2*, a direct target of BMP signaling, were strongly expressed in the interdigital mesenchyme of control hindlimbs at both E12.5 and E13.5. However, the expression of these three genes was profoundly reduced and perturbed in hindlimbs of homozygous mice (Figures 5E–5J). These data suggest that inhibition of apoptosis is spatiotemporally correlated to reduced and/or disturbed expression of genes involved in BMP signaling in the interdigital mesenchyme.

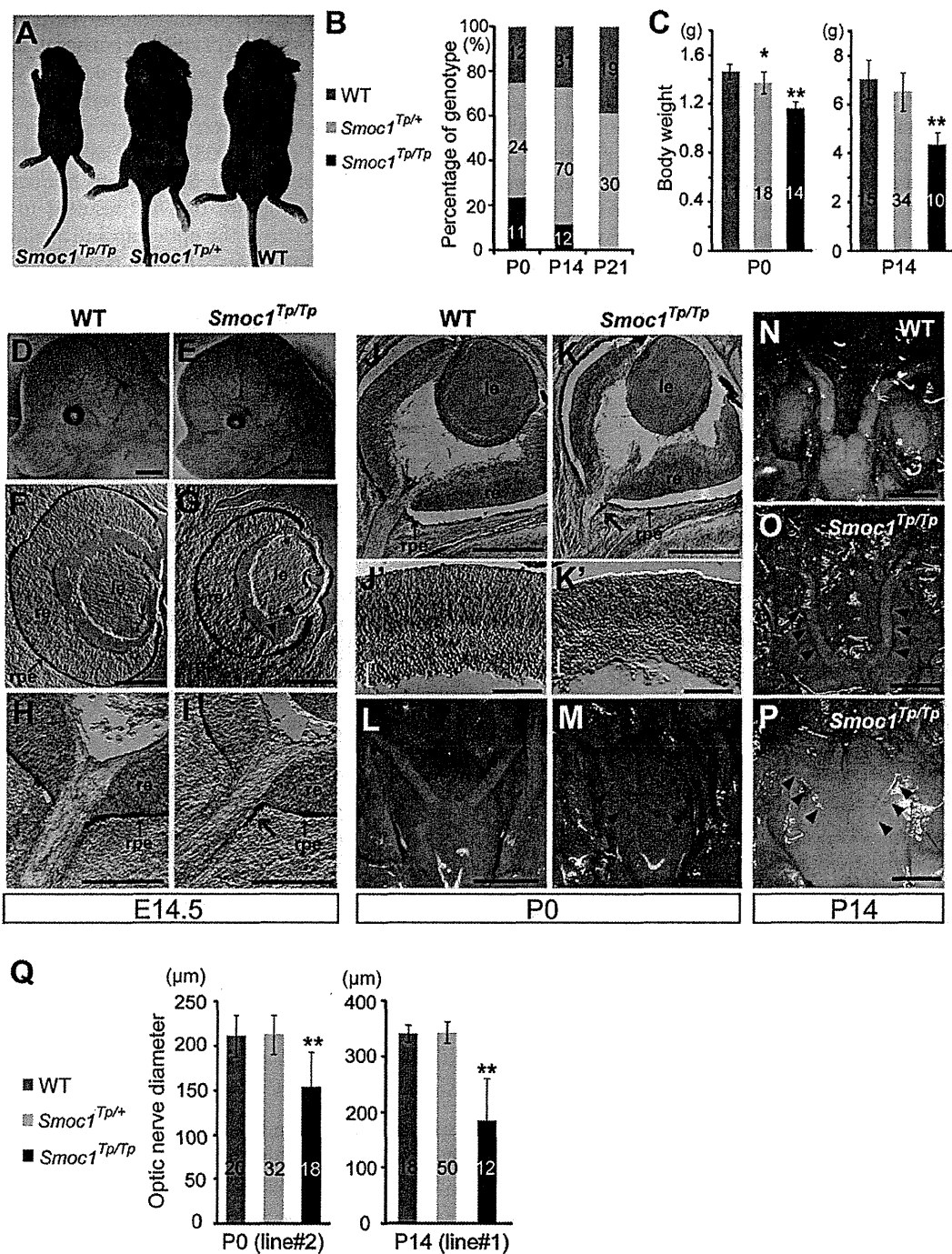


Figure 3. Growth and Ocular Phenotypes of *Smoc1* Null Mice

(A) Representative *Smoc1^{Tp/Tp}* mouse, showing a small body in comparison to *Smoc1^{Tp/+}* and WT littermates.

(B) Genotypes of living pups during the first 3 wk of life.

(C) Body weight of pups of each genotype at P0 (left panel) and P14 (right panel).

(D and E) Relatively small eyes were evident in *Smoc1^{Tp/Tp}* mice in comparison to WT mice.

(F–K') Coronal sections of eyes at E14.5 (F–I) and P0 (J–K') with TB staining (H, I, and J–K'). (F–I) Atrophy of the anteroventral part of the retina (G, magenta arrowheads, dorsal view shown at the top), hypoplastic optic nerve, and extension of the RPE to the optic nerve (I, magenta arrow) in *Smoc1^{Tp/Tp}* mice at E14.5. (J and K) Hypoplastic optic nerve and RPE extension in *Smoc1^{Tp/Tp}* mice at P0 (K, magenta arrow). Note that sections in which optic nerves appeared most thick are presented in (H–K). (J'–K') In higher-magnification views of (J and K), a thinned and irregular ganglion cell layer (white brackets) was observed in *Smoc1^{Tp/Tp}* mice. Abbreviations are as follows: le, lens; re, retina; rpe, retinal pigmented epithelium.

(L–P) Ventral views of the brain showing optic nerves at P0 (L and M) and P14 (N–P), showing various degrees of optic nerve hypoplasia.

Discussion

In a previous report, we performed parametric linkage analysis with three families (families A, B, and C) and found 16 loci showing a LOD score ($\theta = 0.000$) higher than 3.0. Additional microsatellite markers highlighted only one locus, 10p11.23.¹² However, no mutations were found in the candidate gene *MPP7*.¹² By recruiting a new family (family X) to this study, we successfully found homozygous mutations in *SMOC1* in families A, C, and X. In family B, no *SMOC1* mutations were found, indicating the genetic heterogeneity in MLA. Patients with *SMOC1* mutations and *Smoc1* null mice showed similar limb anomalies, such as oligodactyly, syndactyly, synostosis of 4th and 5th metacarpals, hypoplasia of fibula, and bowed tibia. Oligodactyly, syndactyly, and synostosis of 4th and 5th metacarpals are common in MLA patients.²⁻⁴ However, hypoplastic fibula and bowed tibia are less common in patients with MLA, as four out of 34 MLA patients showed these anomalies in the previous report.³ Although one patient with a *SMOC1* mutation from family C did not show bowed tibia and hypoplastic fibula, these anomalies could be features specific to *SMOC1* mutations. Further *SMOC1* analysis of other MLA patients should delineate the phenotypic consequences caused by *SMOC1* mutations.

Accumulating evidence suggests that BMP signaling plays crucial roles in early eye vesicle and limb patterning, skeletal formation, and apoptosis of the interdigital mesenchyme,²⁵⁻²⁹ and mutations involving BMP signaling cause human malformations including ocular, limb, and skeletal anomalies.^{7,30-33} Here, we present genetic evidence that *SMOC1* is essential for ocular and limb development in humans and mice. Furthermore, *Xenopus smoc* can inhibit BMP signaling,¹¹ suggesting that *SMOC1/Smoc1* can also modulate BMP signaling in humans and mice. Indeed, we observed reduced and/or disturbed expression of genes involved in BMP signaling in the interdigital mesenchyme in *Smoc1* null mice, and limb and ocular abnormalities associated with loss of *Smoc1* function are consistent with phenotypic consequences of disturbed BMP signaling. Conditional inactivation of *Bmp2* in the limb showed 3/4 syndactyly, and a similar deficiency of both *Bmp2* and *Bmp7* resulted in malformed fibulae in mice.²⁵ Moreover, mice deficient in *Fmn1*, a repressor of BMP signaling, showed four digits, fused metatarsal bones, and an absence of fibulae in the hindlimbs,³⁴ suggesting the importance of altered BMP signaling in these features. Concerning ocular phenotypes, haploinsufficiency of mouse *Bmp4* resulted in a decreased number of ganglion layer cells and absence of the optic nerve similar to *Smoc1* null mice,³⁵ indicating that altered BMP signaling

is also involved in the ocular phenotype. Interestingly, knockdown experiments of *smoc* by antisense morpholino in *Xenopus* showed absence or severe deformity of the eye and other anterior structures, which were accompanied by aberrant expression of *otx2*, *tbx2* in the eye field.¹¹ Mutations of *OTX2* (MIM 600037) cause microphthalmia, syndromic 5 (MCOPSS [MIM 610125]) in humans.³⁶ Moreover, targeted disruption of *Tbx2* resulted in a marked reduction in the size of the optic cup and a failure of optic nerve formation in mice.³⁷ Thus, it is possible that loss of *SMOC1* function could alter the expression of *OTX2* and *TBX2* (MIM 600747) by disturbing BMP signaling in human developing eyes.

It is unknown how the loss of functional *SMOC1*, a BMP antagonist, leads to reduced expression of genes involved in BMP signaling in the interdigital mesenchyme in *Smoc1* null mice. In the case of *Fmn1*-deficient mice, the loss of the repressor of BMP signaling resulted in downregulation of *Fgf4* and *Shh* and in upregulation of *Gremlin* expression at E10.5, and absence of apoptosis of the interdigital mesenchyme between the two middle digits at E13.5.³⁴ Thus, there is a possibility that loss of *SMOC1* could cause the imbalance among BMP, SHH, and FGF signaling, which would subsequently lead to reduced and/or disturbed expression of genes involved in BMP signaling in the interdigital mesenchyme. In fact, we observed reduced expression of *Msx2* in the progressive zone of hindlimbs at E11.5 (Figure S2). Moreover, expression of *Sox9*, the initial cartilage condensation marker, showed abnormal limb patterning, suggesting that *SMOC1* may affect BMP signaling even at early stages of limb development (Figure S3). Further examinations are required for understanding spatial and temporal actions of *SMOC1/Smoc1* protein during limb development.

In conclusion, our data demonstrate that *SMOC1/Smoc1* is an essential player in both ocular and limb development in humans and mice and give further support to the crucial roles of BMP signaling in these systems.

Supplemental Data

Supplemental Data include three figures and four tables and can be found with this article online at <http://www.cell.com/AJHG/>.

Acknowledgments

We would like to thank the patients and their families for their participation in this study. We thank Yoshiko Takahashi (Nara Institute of Science and Technology) and Atsushi Yamada (Showa University) for providing the *Bmp2* and *Sox9* probes; Elizabeth J. Robertson (University of Oxford) and Makoto Ishibashi (Kyoto University) for the *Bmp7* probe; Robert E. Maxson, Jr. (University of Southern California Keck School of Medicine) for the *Msx2*

(Q) Optic nerve diameter. Optic nerves were significantly hypoplastic in *Smoc1*^{TP/TP} mice in comparison to WT and *Smoc1*^{TP/+} littermates. The numbers of pups (B and C) or eyes (Q) corresponding to each genotype are indicated within bars. Error bars indicate standard deviation: * $p < 0.01$, compared with WT. ** $p < 0.01$, compared with WT and *Smoc1*^{TP/+}. Scale bars represent 1 mm (D, E, and L-P), 200 μ m (F-I), 500 μ m (J and K), and 100 μ m (J' and K').

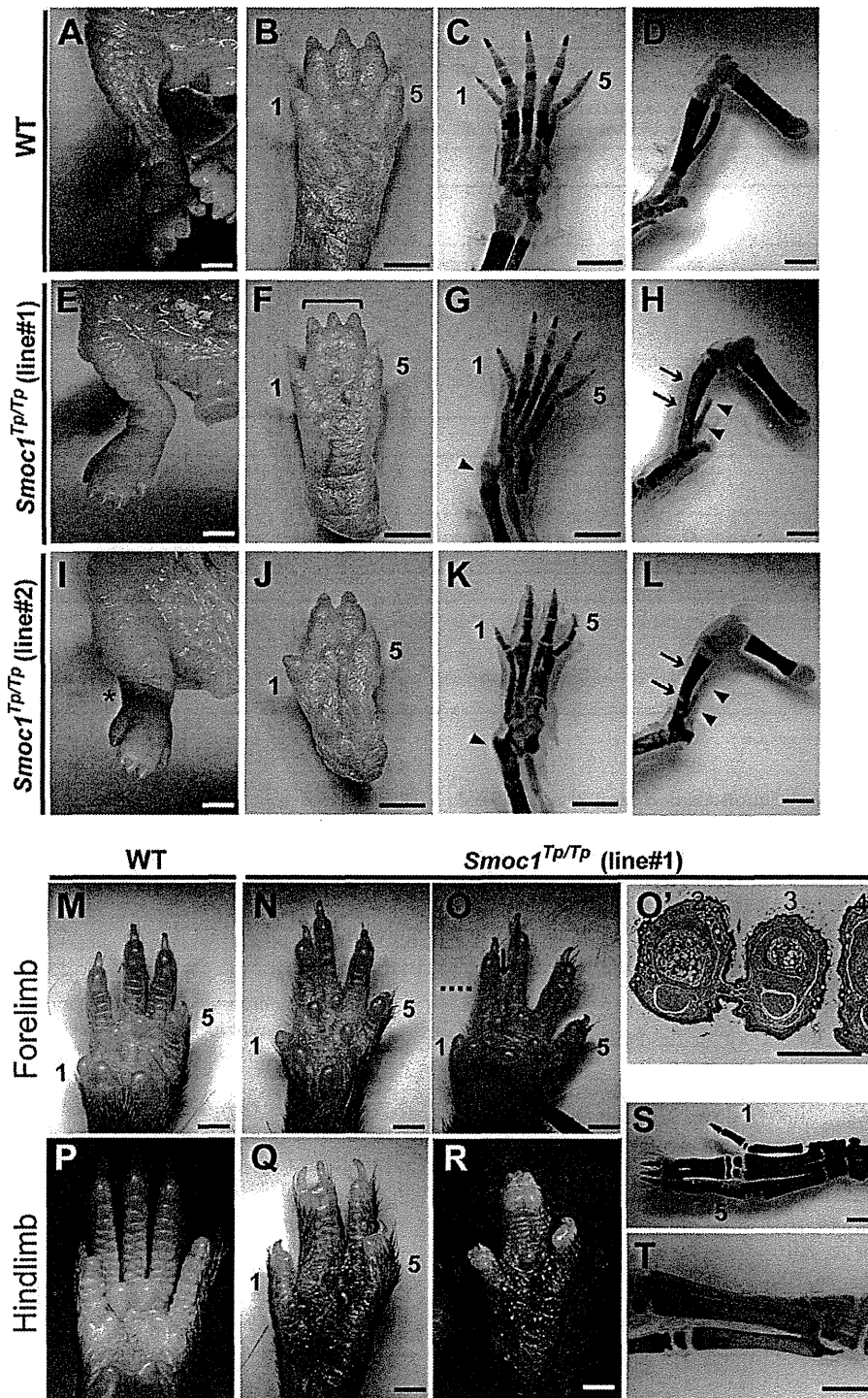


Figure 4. Limb Phenotypes of *Smoc1* Null Mice

Limbs of WT (A–D, M, and P) and *Smoc1^{Tp/Tp}* mice (E–L, N–O', and Q–T) at P0 (A–L) and P14 (M–T). Digit identities are indicated by the numbers 1 (thumb, anterior) and 5 (little finger, posterior). Skeletal staining with alcian blue and alizarin red is presented (C, D, G, H, K, L, S, and T). *Smoc1^{Tp/Tp}* mice showed pes valgus (E and I), soft tissue syndactyly (F and G), and four digits with metatarsal fusion (J and K). Malposition of the articulation between the tibia/fibula and the calcanea (G and K, magenta arrowheads), bowed tibia (magenta arrows), and hypoplastic fibula (arrowheads) of *Smoc1^{Tp/Tp}* mice (H and L) were observed. 2/3 soft tissue syndactyly (N) and 2/3 webbing (O) were evident in forelimbs of *Smoc1^{Tp/Tp}* mice. (O') A transverse section taken at the level indicated by the dashed line in (O) showed 2/3 webbing. 2/3 syndactyly (Q), 2/3/4 syndactyly (R), synostosis between the 2nd and 3rd proximal phalanx and metatarsals (S), and synostosis between the 4th and 5th metatarsals (T, arrow), observed in the hindlimbs of *Smoc1^{Tp/Tp}* mice. Scale bars represent 1 mm (A–O and P–T) or 500 μ m (O').

Table 1. Limb Abnormalities in *Smoc1*^{Tp/Tp} Mutants

Genotype	Talipes Valgus (No. of Affected/ Total No. of Pups)	Forelimb Abnormalities (No. of Limbs)	Hindlimb Syndactyly (No. of Limbs)					Other External Abnormalities (No. of Pups)	4 th and 5 th Metatarsal Fusion (No. of Affected/Total No. of Limbs)
			None	2/3 ^a	3/4 ^b	2/3/4 ^c	4 Digits		
Postnatal Day 0									
<i>Smoc1</i> ^{Tp/+} (line 1, C57BL/6J)	0/42	0	84	0	0	0	0		
<i>Smoc1</i> ^{Tp/+} (line 2, ICR mixed)	0/38	0	76	0	0	0	0		
<i>Smoc1</i> ^{Tp/Tp} (line 1, C57BL/6J)	10/10	0	3	0	3	12	2		
<i>Smoc1</i> ^{Tp/Tp} (line 2, ICR mixed)	13/17	1 ^d	1	1	9	4	19	cleft palate (3)	
Postnatal Day 14									
<i>Smoc1</i> ^{Tp/+} (line 1, C57BL/6J)	0/70	0	140	0	0	0	0		
<i>Smoc1</i> ^{Tp/Tp} (line 1, C57BL/6J)	11/11	18 ^e	2	7	3	8	2	hypoplastic thumbs (5)	9/10 ^f

^a Syndactyly between the 2nd and 3rd digits.
^b Syndactyly between the 3rd and 4th digits.
^c Syndactyly between the 2nd, 3rd, and 4th digits.
^d 2/3 soft tissue syndactyly.
^e Eleven limbs showed 2/3 webbing, four limbs showed 2/3 soft tissue syndactyly, and one limb showed 3/4 syndactyly.
^f Based on examination of skeletal preparations.

probe; Tomonori Hirose, Kazunori Akimoto, and Kazunori Sasaki (Yokohama City University) for providing useful information about mouse breeding, taking photos on a stereo microscope, and mRNA quantification; and Kohei Shiota and Sumiko Kimura (Kyoto University) for helpful comments about NB staining and limb anomalies. This work was supported by research grants from the Ministry of Health, Labour and Welfare (T. Furuichi, N. Miyake, N. Matsumoto, and H.S.) and the Japan Science and Technology Agency (N. Matsumoto), a Grant-in-Aid for Scientific Research from the Japan Society for the Promotion of Science (T. Furuichi and N. Matsumoto), and a Grant-in-Aid for Young Scientist from the Japan Society for the Promotion of Science (K.N., H.D., N. Miyake, and H.S.). This work has been carried out at the Advanced Medical Research Center of Yokohama City University.

Received: September 29, 2010

Revised: November 20, 2010

Accepted: November 26, 2010

Published online: December 30, 2010

Web Resources

The URLs for data presented herein are as follows:

BDGP, <http://www.fruitfly.org/>

ESEfinder 3.0, http://rulai.cshl.edu/cgi-bin/tools/ESE3/ese_finder.cgi?process=home

GenBank, <http://www.ncbi.nlm.nih.gov/Genbank/>

HSF2.4.1, <http://www.umd.be/HSF/>

NetGene2, <http://www.cbs.dtu.dk/services/NetGene2/>

Online Mendelian Inheritance in Man, <http://www.ncbi.nlm.nih.gov/Omim>

UCSC Genome Browser, <http://genome.ucsc.edu/cgi-bin/hgGateway>

SpliceView, <http://zeus2.itb.cnr.it/~webgene/wwwspliceview.html>

References

1. Waardenburg, P.J. (1961). Autosomally-recessive anophthalmia with malformations of the hands and feet. In *Genetics and Ophthalmology*, P.J. Waardenburg, A. Franceschetti, and D. Klein, eds. (Assen, The Netherlands: Royal Van Gorcum), p. 773.
2. Teiber, M.L., Garrido, J.A., and Barreiro, C.Z. (2007). Ophthalmic-acromelic syndrome: report of a case with vertebral anomalies. *Am. J. Med. Genet. A* 143A, 2460–2462.
3. Garavelli, L., Pedori, S., Dal Zotto, R., Franchi, F., Marinelli, M., Croci, G.F., Bellato, S., Ammenti, A., Viridis, R., Banchini, G., and Superti-Furga, A. (2006). Anophthalmos with limb anomalies (Waardenburg ophthalmic-acromelic syndrome): report of a new Italian case with renal anomaly and review. *Genet. Couns.* 17, 449–455.
4. Tekin, M., Tutar, E., Arsan, S., Atay, G., and Bodurtha, J. (2000). Ophthalmic-acromelic syndrome: report and review. *Am. J. Med. Genet.* 90, 150–154.
5. Adler, R., and Canto-Soler, M.V. (2007). Molecular mechanisms of optic vesicle development: complexities, ambiguities and controversies. *Dev. Biol.* 305, 1–13.
6. Zeller, R., López-Ríos, J., and Zuniga, A. (2009). Vertebrate limb bud development: moving towards integrative analysis of organogenesis. *Nat. Rev. Genet.* 10, 845–858.
7. Bakrania, P., Efthymiou, M., Klein, J.C., Salt, A., Bunyan, D.J., Wyatt, A., Ponting, C.P., Martin, A., Williams, S., Lindley, V., et al. (2008). Mutations in BMP4 cause eye, brain, and digit

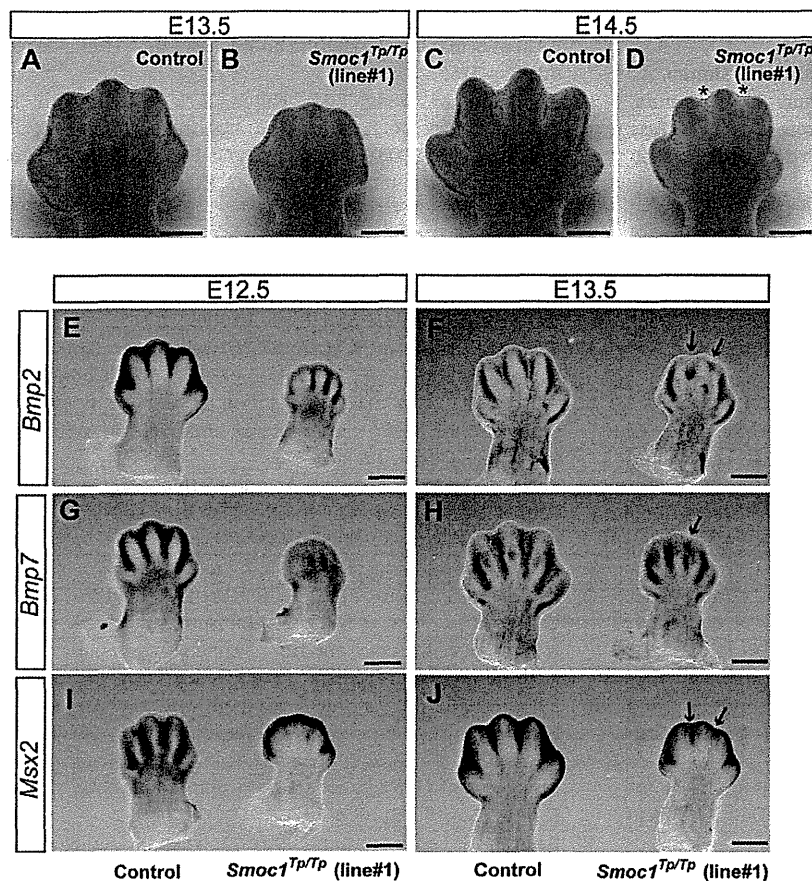


Figure 5. Reduced Apoptosis and Altered BMP Signaling in the Interdigital Mesenchyme of *Smoc1* Null Mice

(A–D) NB staining of left hindlimbs at E13.5 (A and B) and E14.5 (C and D). In comparison to control embryos (WT and *Smoc1*^{Tp/+} littermates) (A and C), the number of NB-stained apoptotic cells in the interdigital mesenchyme of *Smoc1*^{Tp/Tp} mice was dramatically reduced between digits 2 and 3 and digits 3 and 4 at both E13.5 and E14.5, and the webbing remained at a distal level (B and D, magenta asterisk).

(E–J) Whole-mount in situ hybridization of right hindlimbs at E12.5 (E, G, and I) and E13.5 (F, H, and J). At E12.5, interdigital expression of *Bmp2*, *Bmp7*, and *Msx2* was profoundly delayed in the hindlimbs of *Smoc1*^{Tp/Tp} mice, and their expression in the interdigital mesenchyme was apparently perturbed, even at E13.5 (magenta arrows). Scale bar represents 500 μ m.

- developmental anomalies: overlap between the BMP4 and hedgehog signaling pathways. *Am. J. Hum. Genet.* 82, 304–319.
8. Bornstein, P., and Sage, E.H. (2002). Matricellular proteins: extracellular modulators of cell function. *Curr. Opin. Cell Biol.* 14, 608–616.
 9. Vannahme, C., Smyth, N., Miosge, N., Gösling, S., Frie, C., Paulsson, M., Maurer, P., and Hartmann, U. (2002). Characterization of SMOC-1, a novel modular calcium-binding protein in basement membranes. *J. Biol. Chem.* 277, 37977–37986.
 10. Gersdorff, N., Müller, M., Schall, A., and Miosge, N. (2006). Secreted modular calcium-binding protein-1 localization during mouse embryogenesis. *Histochem. Cell Biol.* 126, 705–712.
 11. Thomas, J.T., Canelos, P., Luyten, F.P., and Moos, M., Jr. (2009). *Xenopus* SMOC-1 inhibits BMP signaling downstream of receptor binding and is essential for post-gastrulation development in *Xenopus*. *J. Biol. Chem.* 284, 18994–19005.
 12. Hamanoue, H., Megarbane, A., Tohma, T., Nishimura, A., Mizuguchi, T., Saitu, H., Sakai, H., Miura, S., Toda, T., Miyake, N., et al. (2009). A locus for ophthalmo-acromelic syndrome mapped to 10p11.23. *Am. J. Med. Genet. A.* 149A, 336–342.
 13. Mégarbané, A., Souraty, N., and Tamraz, J. (1998). Ophthalmo-acromelic syndrome (Waardenburg) with split hand and polydactyly. *Genet. Couns.* 9, 195–199.
 14. Cogulu, O., Ozkinay, F., Gündüz, C., Sapmaz, G., and Ozkinay, C. (2000). Waardenburg anophthalmia syndrome: report and review. *Am. J. Med. Genet.* 90, 173–174.
 15. Miyake, N., Kosho, T., Mizumoto, S., Furuichi, T., Hatamochi, A., Nagashima, Y., Arai, E., Takahashi, K., Kawamura, R., Wakui, K., et al. (2010). Loss-of-function mutations of CHST14 in a new type of Ehlers-Danlos syndrome. *Hum. Mutat.* 31, 966–974.
 16. Gudbjartsson, D.F., Thorvaldsson, T., Kong, A., Gunnarsson, G., and Ingólfssdóttir, A. (2005). Allegro version 2. *Nat. Genet.* 37, 1015–1016.
 17. Keng, V.W., Yae, K., Hayakawa, T., Mizuno, S., Uno, Y., Yusa, K., Kokubu, C., Kinoshita, T., Akagi, K., Jenkins, N.A., et al. (2005). Region-specific saturation germline mutagenesis in mice using the Sleeping Beauty transposon system. *Nat. Methods* 2, 763–769.
 18. Mamo, S., Gal, A.B., Bodo, S., and Dinnyes, A. (2007). Quantitative evaluation and selection of reference genes in mouse oocytes and embryos cultured in vivo and in vitro. *BMC Dev. Biol.* 7, 14.
 19. Parr, B.A., Shea, M.J., Vassileva, G., and McMahon, A.P. (1993). Mouse Wnt genes exhibit discrete domains of expression in the early embryonic CNS and limb buds. *Development* 119, 247–261.
 20. Saitu, H., Ishibashi, M., Nakano, H., and Shiota, K. (2003). Spatial and temporal expression of folate-binding protein 1 (Fbp1) is closely associated with anterior neural tube closure in mice. *Dev. Dyn.* 226, 112–117.
 21. Tamplin, O.J., Kinzel, D., Cox, B.J., Bell, C.E., Rossant, J., and Lickert, H. (2008). Microarray analysis of *Foxa2* mutant mouse embryos reveals novel gene expression and inductive roles

- for the gastrula organizer and its derivatives. *BMC Genomics* 9, 511.
22. Suzuki, D., Yamada, A., Amano, T., Yasuhara, R., Kimura, A., Sakahara, M., Tsumaki, N., Takeda, S., Tamura, M., Nakamura, M., et al. (2009). Essential mesenchymal role of small GTPase Rac1 in interdigital programmed cell death during limb development. *Dev. Biol.* 335, 396–406.
 23. Kimura, S., and Shiota, K. (1996). Sequential changes of programmed cell death in developing fetal mouse limbs and its possible roles in limb morphogenesis. *J. Morphol.* 229, 337–346.
 24. Sernagor, E., Eglen, S.J., and Wong, R.O. (2001). Development of retinal ganglion cell structure and function. *Prog. Retin. Eye Res.* 20, 139–174.
 25. Bandyopadhyay, A., Tsuji, K., Cox, K., Harfe, B.D., Rosen, V., and Tabin, C.J. (2006). Genetic analysis of the roles of BMP2, BMP4, and BMP7 in limb patterning and skeletogenesis. *PLoS Genet.* 2, e216.
 26. Robert, B. (2007). Bone morphogenetic protein signaling in limb outgrowth and patterning. *Dev. Growth Differ.* 49, 455–468.
 27. Dudley, A.T., Lyons, K.M., and Robertson, E.J. (1995). A requirement for bone morphogenetic protein-7 during development of the mammalian kidney and eye. *Genes Dev.* 9, 2795–2807.
 28. Khokha, M.K., Hsu, D., Brunet, L.J., Dionne, M.S., and Harland, R.M. (2003). Gremlin is the BMP antagonist required for maintenance of Shh and Fgf signals during limb patterning. *Nat. Genet.* 34, 303–307.
 29. Furuta, Y., and Hogan, B.L. (1998). BMP4 is essential for lens induction in the mouse embryo. *Genes Dev.* 12, 3764–3775.
 30. Asai-Coakwell, M., French, C.R., Berry, K.M., Ye, M., Koss, R., Somerville, M., Mueller, R., van Heyningen, V., Waskiewicz, A.J., and Lehmann, O.J. (2007). GDF6, a novel locus for a spectrum of ocular developmental anomalies. *Am. J. Hum. Genet.* 80, 306–315.
 31. Tassabehji, M., Fang, Z.M., Hilton, E.N., McGaughan, J., Zhao, Z., de Bock, C.E., Howard, E., Malass, M., Donnai, D., Diwan, A., et al. (2008). Mutations in GDF6 are associated with vertebral segmentation defects in Klippel-Feil syndrome. *Hum. Mutat.* 29, 1017–1027.
 32. Wyatt, A.W., Osborne, R.J., Stewart, H., and Ragge, N.K. (2010). Bone morphogenetic protein 7 (BMP7) mutations are associated with variable ocular, brain, ear, palate, and skeletal anomalies. *Hum. Mutat.* 31, 781–787.
 33. Ye, M., Berry-Wynne, K.M., Asai-Coakwell, M., Sundaresan, P., Footz, T., French, C.R., Abitbol, M., Fleisch, V.C., Corbett, N., Allison, W.T., et al. (2010). Mutation of the bone morphogenetic protein GDF3 causes ocular and skeletal anomalies. *Hum. Mol. Genet.* 19, 287–298.
 34. Zhou, F., Leder, P., Zuniga, A., and Dettenhofer, M. (2009). Formin1 disruption confers oligodactylysm and alters Bmp signaling. *Hum. Mol. Genet.* 18, 2472–2482.
 35. Chang, B., Smith, R.S., Peters, M., Savinova, O.V., Hawes, N.L., Zabaleta, A., Nusinowitz, S., Martin, J.E., Davisson, M.L., Cepko, C.L., et al. (2001). Haploinsufficient Bmp4 ocular phenotypes include anterior segment dysgenesis with elevated intraocular pressure. *BMC Genet.* 2, 18.
 36. Ragge, N.K., Brown, A.G., Poloschek, C.M., Lorenz, B., Henderson, R.A., Clarke, M.P., Russell-Eggitt, I., Fielder, A., Gerrelli, D., Martinez-Barbera, J.P., et al. (2005). Heterozygous mutations of OTX2 cause severe ocular malformations. *Am. J. Hum. Genet.* 76, 1008–1022.
 37. Behesti, H., Papaioannou, V.E., and Sowden, J.C. (2009). Loss of Tbx2 delays optic vesicle invagination leading to small optic cups. *Dev. Biol.* 333, 360–372.

CANT1 mutation is also responsible for Desbuquois dysplasia, type 2 and Kim variant

Tatsuya Furuichi,^{1,2} Jin Dai,¹ Tae-Joon Cho,³ Satoru Sakazume,⁴ Masahide Ikema,⁵ Yoshito Matsui,⁶ Gareth Baynam,⁷ Toshiro Nagai,⁴ Noriko Miyake,⁸ Naomichi Matsumoto,⁸ Hirofumi Ohashi,⁹ Sheila Unger,¹⁰ Andrea Superti-Furga,¹⁰ Ok-Hwa Kim,¹¹ Gen Nishimura,¹² Shiro Ikegawa¹

► Additional figures and tables are published online only. To view these files please visit the journal online (<http://jmg.bmj.com>).

¹Laboratory of Bone and Joint Diseases, Center for Genomic Medicine, RIKEN, Tokyo, Japan

²Laboratory Animal Facility, Research Center for Medical Sciences, Jikei University School of Medicine, Tokyo, Japan

³Department of Orthopaedic Surgery, Seoul National University Children's Hospital, Seoul, Korea

⁴Department of Pediatrics, Dokkyo Medical University Kosigaya Hospital, Koshigaya, Japan

⁵Department of Orthopaedic, Nagasaki Prefectural Center of Medicine and Welfare for Children, Nagasaki, Japan

⁶Department of Orthopedic Surgery, University of Toyama, Toyama, Japan

⁷Genetic Services of Western Australia, Princess Margaret Hospital for Children and King Edward Memorial Hospital for Women, Western Australia, Australia

⁸Department of Human Genetics, Yokohama City University Graduate School of Medicine, Yokohama, Japan

⁹Division of Medical Genetics, Saitama Children's Medical Center, Iwatsuki, Japan

¹⁰Center for Pediatrics and Adolescent Medicine, University of Freiburg, Freiburg, Germany

¹¹Department of Radiology, Ajou University Hospital, Suwon, Korea

¹²Department of Pediatric Imaging, Tokyo Metropolitan Children's Medical Center, Fuyu, Japan

Correspondence to

Dr Shiro Ikegawa, Laboratory of Bone and Joint Diseases, Center for Genomic Medicine, RIKEN, 4-6-1 Shirokanedai, Minato-ku, Tokyo 108-8639, Japan; sikegawa@ims.u-tokyo.ac.jp

Received 8 May 2010

Revised 30 June 2010

Accepted 3 July 2010

Published Online First

30 October 2010

ABSTRACT

Background Desbuquois dysplasia (DD) is a recessively inherited condition characterised by short stature, generalised skeletal dysplasia and advanced bone maturation. DD is both clinically and radiographically heterogeneous, and two subtypes have been distinguished based on the presence (type 1) or absence (type 2) of an accessory metacarpal bone. In addition, an apparently distinct variant without additional metacarpal bone but with short metacarpals and long phalanges (Kim variant) has been described recently. Mutations in the gene that encodes for CANT1 (calcium-activated nucleotidase 1) have been identified in a subset of patients with DD type 1.

Methods A series of 11 subjects with DD from eight families (one type 1, two type 2, five Kim variant) were examined for CANT1 mutations by direct sequencing of all coding exons and their flanking introns.

Results Eight distinct mutations were identified in seven families (one type 1, one type 2 and all 5 Kim variant): three were nonsense and five were missense. All missense mutations occurred at highly conserved amino acids in the nucleotidase conserved regions of CANT1. Measurement of nucleotidase activity in vitro showed that the missense mutations were all associated with loss-of-function.

Conclusion The clinical-radiographic spectrum produced by CANT1 mutations must be extended to include DD type 2 and Kim variant. While presence or absence of an additional metacarpal ossification centre has been used to distinguish subtypes of DD, this sign is not a distinctive criterion to predict the molecular basis in DD.

INTRODUCTION

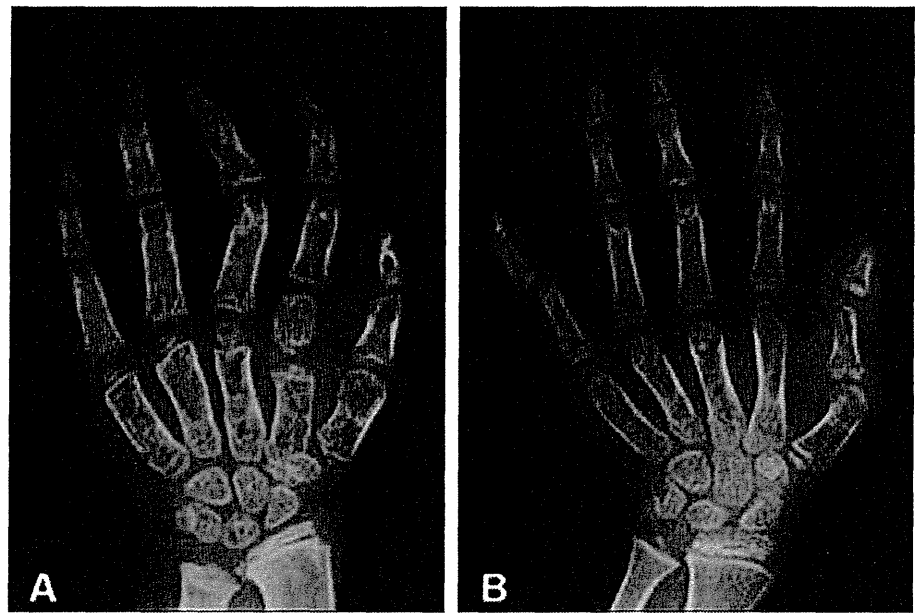
Desbuquois dysplasia (DD; MIM 251450) is a severe skeletal dysplasia inherited in an autosomal recessive manner. DD belongs to the 'multiple dislocation group' in the International Nosology of Genetic Skeletal Disorders.¹ It is characterised clinically by short limb short stature, severe joint laxity with facultative congenital dislocations, flat midface, microgathia, cleft palate, and progressive scoliosis. The main radiological features include a peculiar 'monkey wrench' or 'Swedish key' appearance of the proximal femur (exaggerated trochanter), hypoplasia of thorax and ilia, mild spondylar dysplasia, and hand abnormalities including an additional ossification centre and advanced bone age.²

DD has been considered clinically and radiographically heterogeneous. It has been classified into two types on the basis of the presence (type 1) or absence (type 2) of characteristic hand anomalies, which consist of an extra ossification centre distal to the second metacarpal, delta phalanx, bifid distal thumb phalanx, and dislocation of the interphalangeal joints (figure 1A).³ DD type 2 is also referred to as the 'normal' hand type because the accessory metacarpal ossification centre is not seen. It only presents with minor changes of the hand, such as malalignment of the interphalangeal joint and brachydactyly. More than half of the DD patients belong to this subtype.³ In addition, we have recently described a new clinical subtype of DD, Kim variant.⁴ The hand shape of the variant is apparently normal, thus the patients most closely resemble type 2; however, the radiographic abnormalities in the hands are significant, including short metacarpals and elongated phalanges together with remarkably advanced carpal bone age (figure 1B). Long term follow-up showed that severe precocious osteoarthritis of the hand and spine is a major manifestation of this specific clinical variant.⁴

The apparent phenotypical heterogeneity of DD has been taken to suggest genetic heterogeneity. Thus, the DD gene was localised to a 1.65 Mb interval on chromosome 17q25 by homozygosity mapping using four consanguineous families with DD type 1, while DD with normal hands was believed not to map to this interval.^{5,6} Recently, Huber and colleagues searched for mutations in genes in the interval and identified mutations in the calcium activated nucleotidase 1 (CANT1) gene.⁷ CANT1 is a extracellular protein that functions as a nucleotide tri- and diphosphatase. It preferentially hydrolyses uridine diphosphate (UDP) followed by guanosine diphosphate (GDP), uridine triphosphate (UTP) and adenosine diphosphate (ADP).⁸⁻¹⁰

The function of CANT1 in skeletal formation is unknown. It is expressed in chondrocytes, and chondrocytes from DD type 1 patients with CANT1 mutations have abnormally distended rough endoplasmic reticulum (ER) implicating CANT1 in chondrocyte ER metabolism.⁷ The disease-causing mechanism of CANT1 mutation is also unclear. The first mutation study reported seven CANT1 mutations; three are nonsense mutations that are predicted to cause the nonsense mutation mediated RNA decay and one is a homozygous large deletion encompassing 5'-UTR and exon 1 that results in loss of CANT1 mRNA.⁷

Figure 1 Hand radiographs of Desbuquois dysplasia (DD) type 1 and Kim variant at age 3 years. (A) DD type 1 carrying the homozygous *CANT1* mutation, p.R300C. This girl has been reported previously as family 4.⁷ Note the additional ossification centre at the second metacarpal. (B) DD Kim variant (patient 7 in the present study) carrying the compound heterozygous *CANT1* mutations, p.V226M and p.A360D. There is no additional ossification centre. Both patients show precocious carpal ossification.



These findings suggest that loss of *CANT1* function causes DD. However, functional impact of the missense mutations has not been examined. It is of note that the genetic mapping was done using DD type 1 families, and that all patients in whom *CANT1* mutations were identified had DD type 1.⁷ Therefore, it remains to be determined whether *CANT1* is responsible for other types of DD.

To explore further the range of *CANT1* mutations in DD, we searched for *CANT1* mutations in three types (type 1, type 2, Kim variant) of DD patients. We found a total of eight distinct mutations in seven families (type 1, type 2, and all five Kim variant); all were novel. By measuring the *CANT1* enzyme activity in vitro, we confirmed that DD results from *CANT1* loss of function.

PATIENTS AND METHODS

Patients

DD patients were recruited through the International Skeletal Dysplasia Registry (ISDR) (<http://www.csmc.edu/>), the European Skeletal Dysplasia Network (ESDN) (<http://www.esdn.org/>), and the Japanese Skeletal Dysplasia Consortium (JSDC) (<http://www.riken.jp/lab-www/OA-team/JSDC/>). Clinical criteria for inclusion in the study were prenatal and postnatal growth failure with short limbs, mid-face hypoplasia or round face with flat nasal bridge, joint laxity and foot deformities. Major radiological criteria were Swedish key appearance of the proximal femur, advanced carpo-tarsal ossification, short tubular bones, and hyperphalangy (extra-ossicle between the proximal phalanx and metacarpal of the index finger) in type 1. Minor radiological criteria included hypoplastic lower ilia and vertebral modification, such as coronal clefts or irregular endplates at birth and mild vertebral flattening with round vertebral endplates or normal vertebral bodies in later life. Clinical and radiographic phenotypes of the patients were evaluated by the experts of the organisations and reviewed by the authors (SU, AS-F, OK, and GN).

Eleven patients with DD from eight families were recruited for this study (table 1). Clinical data of patient 1 have been reported previously.¹¹ Patients 4, 5, 7, and 8 have also been

reported previously (as patients 3, 5, 6, and 1, respectively).⁴ The study was approved by the ethics committee of RIKEN and participating institutions and informed consent was obtained from all subjects.

Mutation screening

Genomic DNA was extracted from blood by standard procedures or from saliva using Oragene DNA Self-Collection kit (DNA Genotek, Kanata Ontario, Canada). Exon sequences of *CANT1* with their flanking intron sequences were amplified by PCR from genomic DNA. PCR primer sequences and PCR condition are listed in supplemental table 1. PCR products were purified using MinElute PCR purification Kit (Qiagen, Valencia, CA, USA) and sequenced for both strands using an ABI Prism 3730 automated sequencer (PE Biosystems, Foster City, CA, USA). Genomic DNAs from the parents and sibs were sequenced for the corresponding regions.

cDNA cloning and in vitro mutagenesis

The full length *CANT1* cDNA was amplified by PCR using cDNAs prepared from OUMS-27 cells as a template and cloned into pcDNA3.1 (+). The missense mutations were introduced into *CANT1* cDNA by PCR based mutagenesis. The introduced mutations were confirmed by DNA sequencing.

Nucleotidase assay

COS-7 cells were grown to 70–80% confluence in 100 mm culture dishes and were transfected with 6 µg of empty, wild-type or mutant *CANT1* expression vectors using Fugene 6 transfection reagent (Roche Diagnostics, Basel, Switzerland). At 8 h after transfection, cells were transferred to Opti-MEM serum-free media and cultured for 48 h. Buffer exchange in the culture supernatant (10 ml) was performed with ultrafiltration through Amicon Ultra-10K centrifugal filter (Millipore, Billerica, MA, USA) using 50 ml of sterile deionised water and the resulting solution concentrated to 100 ml using VIVASPIN 500, 10000 MWCO (Vivascience, Hanover, Germany). Nucleotidase activities in the purified media were determined by modification of a previous method.¹² Briefly, the purified media were 20 times or 500 times diluted with 40 mM succinate buffer (pH 6.5)